

Detection of Biomarkers through Functionalized Polymers

Litzzy L. García-Faustino, Stephen M. Morris, Steve J. Elston, and Yunuen Montelongo*

Over the past decade, there has been a rising interest in utilizing functionalized porous polymers for sensor applications. By incorporating functional groups into nanostructured materials like hydrogels, nanosheets, and nanopores, exciting new opportunities have emerged for biomarker detection. The ability of functionalized polymers to undergo physical changes and deformations makes them perfect for modulating optical signals. This chemical mechanism enables the creation of biocompatible sensors for in situ biomarker measurement. Here a comprehensive overview of the current publication trends is provided in functionalized polymers, encompassing functional groups that can induce measurable physical deformations. It explores various materials categorized based on their detection targets, which include proteins, carbohydrates, ions, and deoxyribonucleic acid. As such, this work serves as a valuable reference for the development of functionalized polymer-based sensors.

converts a physical measure into a signal that is read by an observer or by an instrument.^[16] In this context, an ideal biosensor should be capable of creating an accurate, repeatable, and reproducible physical signal in the presence of analytes.^[17] Biosensors have been utilized to detect and quantify diverse biological components such as nucleic acids (Deoxyribonucleic acid (DNA), RNA, etc.),^[18–20] proteins (antibodies, enzymes, etc.),^[21] as well as other biomolecules (carbohydrates, lipids, peptides, metabolites, etc.).^[22–24] The development of novel photonic biosensors has boosted the exploration of diverse families of biocompatible materials, such as polymers. Polymers are ideal materials for their capability to create porous structures, optical transmittance, mechanical

1. Introduction

In recent years polymer science has become an immense multidisciplinary field involving different subfields, from synthetic polymers, biopolymers, polymer characterization, and design to the manufacturing of new innovative products.^[1] Since the development of the first cross-linking techniques in the 1920s, polymers have transformed human life with the development of materials for environmental sustainability,^[2,3] biomedical applications, aerospace development,^[4–6] and food industry.^[7–9] Particularly, there is a growing interest in the application of polymers in the area of photonics^[10–13] and sensors,^[14,15] where these materials have paved the way for the in vivo detection of biomarkers. In general terms, a sensor can be conceived as a device that

elasticity, and more importantly sensitivity to external stimuli. Such stimuli can produce changes in both physical properties and chemical structure. Some typical environmental stimuli include pH, temperature, ionic strength, light irradiation, mechanical forces, specific analytes, or external additives (ions, bioactive molecules, etc.).^[25]

Although most structural changes are irreversible in these materials, there is a particular interest in reversible alterations that can be tracked and quantified in real time. The incorporation of functional groups in polymers has opened new avenues for the creation of reversible and selective physical interactions in the presence of biomarkers. As shown in **Figure 1A**, the most common approaches related to protein detection are hydrogels, nanosheets, and nanopores, which bring selectivity for the protein to be analyzed. For carbohydrate detection, various structured elements such as nanoantennas and hydrogels have been implemented. Conversely, in the field of ion detection, nanotechnology is witnessing a growing trend with the utilization of carbon nanotubes (CNTs), nanofibers, nanobelts, and microspheres. Finally, in the case of DNA, the main approaches are related to DNA origami and other methods such as surface-enhanced Raman spectroscopy (SERS) and microcapillaries. According to the Scopus database,^[26] the number of articles published on topics related to the detection of proteins, carbohydrates, ions, and DNA and polymers as a whole has had a gradual and steady growth for more than a decade, being 2021 the year where more publications (**Figure 1B**).

Biomarker sensors have become an elementary tool for disease management in modern medicine, leading to a substantial increase in the number of published articles over the past decade. However, to ensure continued progress in this area, it is crucial to

L. L. García-Faustino
School of Engineering and Sciences
Tecnológico de Monterrey
Ave. Eugenio Garza Sada 2501, Monterrey, NL 64849, Mexico
S. M. Morris, S. J. Elston, Y. Montelongo
Department of Engineering Science
University of Oxford
Parks Road, Oxford OX1 3PJ, UK
E-mail: yunuen.montelongo@eng.ox.ac.uk

The ORCID identification number(s) for the author(s) of this article can be found under <https://doi.org/10.1002/smt.202301025>

© 2023 The Authors. Small Methods published by Wiley-VCH GmbH. This is an open access article under the terms of the Creative Commons Attribution-NonCommercial-NoDerivs License, which permits use and distribution in any medium, provided the original work is properly cited, the use is non-commercial and no modifications or adaptations are made.

DOI: 10.1002/smt.202301025

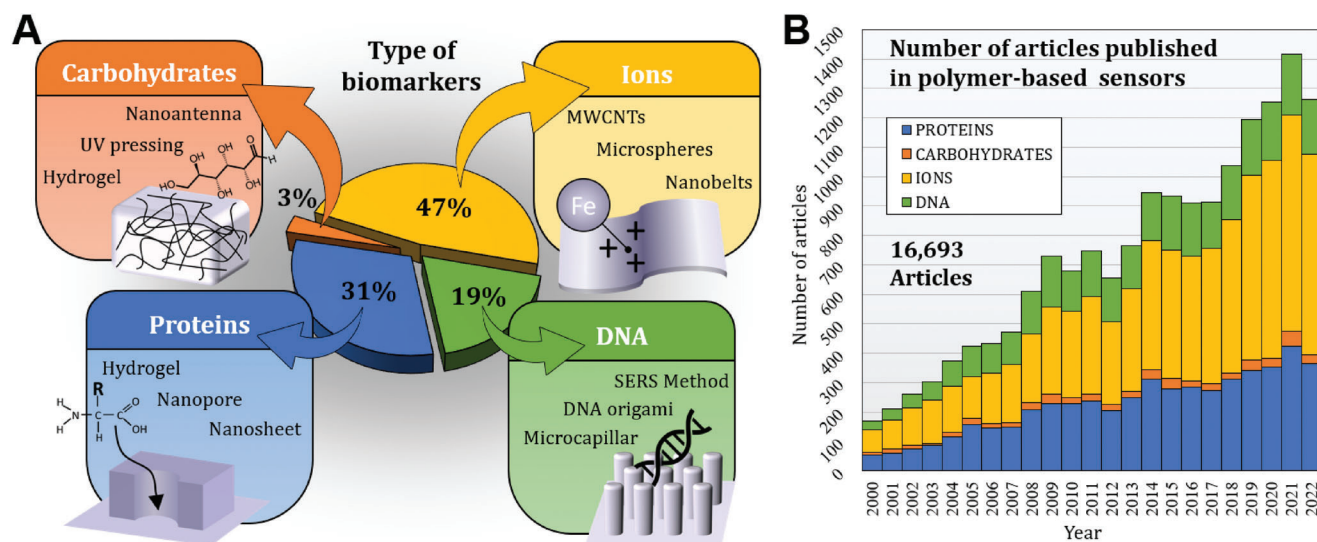


Figure 1. Classification and impact of polymers for detection of biomarkers. A) Classification of polymeric sensors and techniques based on target biomarkers. This includes polymers for the detection of proteins, carbohydrates, ions, and DNA (the percentage of literature published for sensors from the Scopus database has been added as a reference of impact). B) Distribution of published articles, and the current trends in the development of sensors in the range of years from 2000 to 2022 (Scopus database). The plot is divided by target biomarker in each year. A clear increment in polymer-based sensors can be observed for the four types of biomarker studied.

prioritize the revision and classification of these articles.^[27,28] In this comprehensive study, we performed an extensive review of the most recent and cutting-edge scientific literature. The main objective of this work is to establish a systematic classification by type of biomolecules. This classification of biomarkers includes carbohydrates, proteins, metal ions, and DNA. This review focuses specifically on classifying biomarkers rather than serving as a mere glossary of techniques. It aims to be a reference in sensing mechanisms, with a primary focus on the target biomarker. Throughout the review, each section expands on the extensive range of techniques and protocols available (as shown in Table 1).

2. Protein Detection

Proteins are large molecules consisting of amino acid chains. There are a total of 20 different amino acids found in the human body; however, there are hundreds to thousands of bound combinations that create the 3D long chains found in biological tissues.^[29] Depending on their specific purpose, they present various functional group arrangements, which include alcohols, thiols, thioethers, carboxylic acids, carboxamides, and a variety of basic groups.^[30] Proteins are not only found in tissues, they also have an active role in a wide range of biological processes such as assisting in metabolism, providing structural support, and acting as enzymes, carriers, or hormones. In addition, they function as catalyzers, carriers, and depositories of other molecules (such as oxygen), provide mechanical support and immune protection, generate movement, transmit nerve impulses, and control growth and differentiation.^[30]

The malfunctioning of metabolic processes is usually linked to alterations either in the protein concentration or their molecular structure. Hence, the accurate detection of proteins can elucidate the molecular basis of various diseases, which in turn can provide information on prevention, diagnosis, and treatment.^[31]

In the early history of protein detection, Wu proposed the use of Folin phenol reagent,^[32] but later, more methods were adopted by A. G. Gornall. For example, he published the Biuret method which is based on the dependence of the components of the reagents for the determination of serum protein.^[33] In recent years, the process of detection of specific proteins includes the direct monitoring of molecular interaction, gel electrophoresis, and parallelized enzyme-linked immunosorbent assay (ELISA), among others. Furthermore, protein detection has been expanded to new areas with the use of chemical and physical routes, e.g., hydrogels and nanopores as permeable bare bones for the detection and quantification of proteins. Cai et al. introduced a novel sensor based on hydrogel to detect lectin proteins. They utilized a 2D photonic crystal (PC) to monitor the shift in diffraction when the hydrogel was attached to the 2D PC.^[34] Lectins are multivalent sugar-binding proteins of a non-immune nature, which do not exhibit enzymatic activity toward their sugar ligands. In the process, carbohydrates are not chemically modified or metabolized by them, although they bind reversibly in the presence of specific carbohydrates.^[35] Also, Cai et al. demonstrated a copolymerization of a vinyl-bonded carbohydrate monomer with acrylamide (AAm) and acrylic acid (AAc) to fabricate a carbohydrate hydrogel. The sensor developed was made with carbohydrate monomers such as 2-allylethoxyl- β -D-lactose and 2-allylethoxyl- α -D-lactose. These carbohydrates are bound to the polymer skeleton, which binds in a multivalent way to lectin proteins. In addition, a 2D colloidal photonic crystal matrix of solutions of 50 μ L AAm, AAc, *N*'-methylene-bis-(acrylamide) (MBAAm), and carbohydrate monomer was utilized, but other monomers such as 2-allylethoxyl- β -D-lactose and 2-allylethoxyl α -D-mannose were also tested. The 2D PC supports the quantification of the lectin proteins using a monolayer array. In this work, copolymerization was carried out via exposure to 365 nm UV light. To study their behavior with the different

Table 1. Extensive list of techniques and protocols.

Type of sensor	Biomarker	Functional group	Polymer	Year of publication	Reference
PROTEINS					
Carbohydrate–protein recognition sensor	Lectin proteins (ricin, jacalin)	Carbohydrates (lactose, galactose, mannose)	PAAm–AAC–carbohydrate	2017	[34]
Carbohydrate–protein recognition sensor	Lectin–concanavalin A	Metal binding	AAm, AAC, MBAAm, monomer Man-1	2014	[36]
Carbohydrate–protein recognition sensor	Concavalin A/wheat germ agglutinin	Saccharide groups	Glycosylated peptoids	2018	[38]
Antigen–antibody sensor	Human serum albumin antigen	Carboxylic groups	PMMA–parylene-C	2021	[40]
Terahertz biosensor	Bovine serum albumin	–	Stainless steel–no polymer	2021	[46]
Terahertz biosensor	Avian Influenza (AI) viruses	–	Au–no polymer	2017	[1]
Terahertz biosensor	Avidin–AuNPs	Refractive index	Au/SU-8	2016	[50]
Terahertz biosensor	Epidermal growth factor receptor (EGFR) protein	EGFR antibody	Au–no polymer	2018	[49]
Terahertz biosensor	AI viruses (H5N2, H1N1, H9N2)	Refractive index	Au–no polymer	2018	[51]
Terahertz biosensor	α -thrombin (h-TB)	Aptamers (S1) (S2)	(PAm)-(S1) (S2)	2021	[52]
Molecular recognition sensor	Immunoglobulin G1 (IgG), bovine serum albumin (BSA), and streptavidin	Nanopore	PEG–Dimethylacetamide (DMA)	2020	[56]
Electric hybrid sensor	Phosphonate-binding protein (PhnD)	NHS group	P(DMAA-co-NMAs)	2020	[60]
CARBOHYDRATES					
Terahertz biosensor	Glucose	Boronic acid groups	Poly(HEMA-EGDM-AAPBA)	2021	[71]
Photonic bandgap sensor	Glucose	Boronic acid groups	PAAm–polystyrene NPs	2018	[65]
2D photonic crystal hydrogel sensor	Glucose	Boronic acid–boronate	4-butyl boronic acid-Poly(vinyl alcohol) (4-BBA–PVA)–polystyrene NPs	2018	[66]
Chemiresistive sensor	Glucose	Glucose oxidase (GOx)	P4VP-Single-walled carbon nanotubes (SWCNTs)-GOx	2017	[67]
Electrochemical sensor	Glucose	Glucose oxidase (GOx)	Silicon-on-insulator (SOI)–GOx–No polymer	2019	[68]
Wireless patch-type glucose sensor	Glucose	Glucose oxidase (GOx)	Hyaluronate (HA)–AuNP/GOx	2019	[69]
Enzyme-based microcantilever sensor	Glucose	Glucose oxidase (GOx)	GOx–Poly(ethyleneimine) (PEI)–Poly(sodium-p-styrenesulfonate) (PSS)	2005	[70]
Plasmonic sensor	Glucose	Boronic acid groups	Poly(HEMA–EGDM–AAPBA)	2015	[71]
Quartz crystal microbalance (QCM) sensor	Glucose	Boronic acid–boronate	3-APB-BIS-AM-DMPA	2020	[72]
Molecularly imprinted (MIP) sensor	Fructose	Boronic acid groups	β -D-fructopyranose 2.3: 4,5-bis-O-((4-vinylphenyl)boronate)	2008	[84]
Quartz crystal microbalance (QCM) sensor	Fructose	Boronic acid groups (Lewis acid)	(PS- <i>b</i> -P2VP)	2013	[92]
1D photonic crystal sensor	Fructose	D-Fructose dehydrogenase	Osmium redox polymer	2014	[142]

(Continued)

Table 1. (Continued)

Type of sensor	Biomarker	Functional group	Polymer	Year of publication	Reference
Electrochemical sensor	IONS				
	Ca ²⁺	K ⁺ /carboxylic group (COO—K ⁺)	Acetone/KOH-treated poly(acrylic acid) (PAA)	2019	[99]
Optical ion sensor	Ca ²⁺ and Mg ²⁺ in human saliva and serum	K ⁺ /carboxylic group (COO—K ⁺)	KOH/PAA	2021	[100]
Pdot sensor	Cu ²⁺ and Fe ²⁺	Carboxyl groups	PS-COOH-co-PFBT Pdots	2011	[102]
Metal-ion recognition	Mg ²⁺	—	Conjugated polyelectrolyte/Multi-Walled Carbon Nanotube (M/poly(pyrrole) (CPE-K/MWCNT/PPY)	2020	[103]
BODIPY-colorimetric fluorescent chemosensor	Fe ³⁺	Phenol groups	BODIPY-No polymer	2015	[98]
Electrochemical sensor	Fe ³⁺	Ketone	Curcumin-Zein	2019	[104]
Cationic sensor	Cu ²⁺	Alkyl-S1 and azido-S2	Polystyrene	2018	[111]
DNA-based nanopore sensor	Circular plasmid New England Biolabs (pNEB)	Graphene nanoribbon (NR)	Graphene NR-SiNx-No polymer	2013	[122]
DNA-based nanopore sensor	dsDNA	Nanopore	SiN-No polymer	2008	[124]
DNA-based nanopore sensor	ssDNA-dsDNA	Graphene nanopore	Graphene-No polymer	2013	[125]
DNA origami sensor	ssDNA	DNA origami nanopore	DNA origami	2013	[126]
Metal-ion recognition Sensor	DNA bases	T bases	DNA origami	2016	[130]
DNA origami sensor	dsDNA	Carboxylate groups	PVA	2018	[131]
Nanopore—nanofiber mesh biosensor	dsDNA	Nanopore—nanofiber mesh	Poly(glycerol monostearate-co-ε-caprolactone) (PCL)—poly(glycerol monostearate-co-ε-caprolactone) (PGC-C18)	2013	[134]
Nanopore sensor	dsDNA	Solid-state nanopore	Nanoporous silicon nitride (NPN) membrane	2018	[132]
Nanopore sensor	dsDNA	(SiN) nanopore	Agarose gel	2015	[133]
Electrochemical sensor	ssDNA	Peptidomimetic neutral amide bonds	Peptide nucleic acid (PNA)	2007	[141]
Colorimetric sensor	dsDNA	Carbohydrates histidine, lysine, and glutamate	DOPA-X dipeptides	2020	[137]
Ionic current sensor	PCR-amplified gene markers for <i>E. coli</i> O157:H7 (rfbO157, rfbO157, eae, vt1, and vt2)	Oligonucleotide	Zeonor	2021	[138]
Electrochemical sensor	complementary DNA (DNAC)	Azido-DNA	Poly-L-lysine (PLL)-oligo(ethylene glycol) (OEG)-dibenzocyclooctyne (DBCO)	2020	[143]
Colorimetric sensor	Target DNA	Thiol-modified DNA	PAAm-acrylate DNA-DNA AuNPs	2010	[135]
SERS-based sensor	ssDNA ³	Sugar—phosphate linkages	PNAs-AgNPs-R6G	2007	[141]

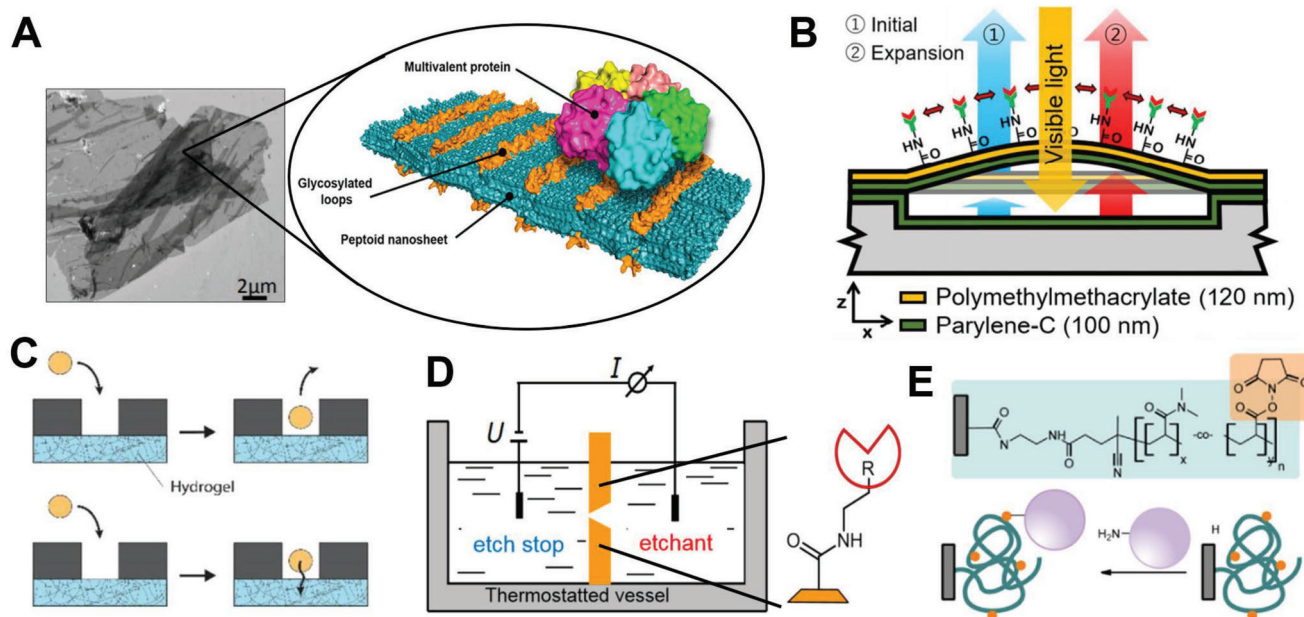


Figure 2. Various techniques implemented for protein detection. A) Nanosheet of glycosylated peptides for protein detection. Reproduced with permission.^[38] Copyright 2018, American Chemical Society. Peptides offer the advantage of improved control over the monomer sequence, enabling them to mimic the cell membrane by self-assembling into nanosheets. B) Immunosensor MEMS based on optical interferometry. Reproduced with permission.^[40] Copyright 2021, Elsevier. The device consists of a microcavity built between a deformable membrane of PMMA and parylene C, and a silicon substrate. C) Mechanism for the detection of proteins based on nanopores and hydrogel. Reproduced with permission.^[56] Copyright 2020, American Chemical Society. The hydrogel located on the distal side of the nanopore sterically interacts with the translocation of native proteins. D) Fabrication of nanopores in the polymer sheet and its functionalization through carboxyl groups. Reproduced with permission.^[43] Copyright 2017, the Authors. Here, chemical etching of a polyester structure is utilized to create a terminal carboxyl group on the surface of the nanopore due to hydrolysis. E) Recognition of phosphonates through the pH alteration in the polymer binding P(DMAA-co-NMAS). Reproduced with permission under the terms of the Creative Commons CC BY license.^[60] Copyright 2020, the Authors. Published by American Chemical Society. A hybrid electric nanosensor utilized a bacterial SBP protein to bind a solid-state nanopore. A stream dependent on both, the concentration of proteins and the ligand interactions with the protein, is created in this process.

lecithin proteins (ricin, jacalin, and concanavalin A (Con A)), optical diffraction was performed, where the wavelengths varied in the full visible spectrum. The optical signal showed a correlation between the contraction of each type of carbohydrate monomer and the type of protein utilized. The 2D PC PAAm–AAc–lactose sensor selectively detects ricin and shows a ricin detection limit of $9 \mu\text{g mL}^{-1}$. The α -galactose hydrogel sensor is selective for jacalin (limit of detection (LoD) = $2.3 \times 10^{-7} \text{ M}$), while the mannose hydrogel sensor is highly selective for Con A (LoD = $3.8 \times 10^{-8} \text{ M}$).

Using the same principle of UV copolymerization, various investigations have reported the successful detection of lectins. Zhang et al., developed a sensor for the detection of lectin Con A through the use of mannose monomers (Man-1).^[36] First, colloidal 2D polystyrene arrays were placed on a glass slide in which layers of AAm, AAc, MBAAM, and Man-1 solutions were deposited. Later, the polymerization process was carried out with UV light (365 nm). The process of binding mannose and Con A occurs by its four identical subunits. Each subunit has a particular saccharide-binding site, and two binding sites for two different metals (Ca^{2+} and transition metals such as Ni^{2+} and Mg^{2+}).^[37] All mannoses are bound to Con A by hydrogen bonding and van der Waals interactions. Once the mannose hydrogel is joined with Con A, the formed cross-links shrink the hydrogel, causing a blueshift in the optical diffraction. It was shown that in the ab-

sence of Con A the shift was 600 nm and, with the presence of Con A, this was 554 nm. Of the various tests that were done to determine the best amounts of polymer, the best sensor M2 (characterized for a 1080 nm of particle spacing) presented a detection limit of 0.02 mg mL^{-1} ($0.7 \mu\text{M}$). In this case, its reversibility was also demonstrated with five cycles of use.

Other mechanisms involving the detection of lectins, such as the implementation of nanosheets, have had increasing attention in recent years. Battigelli et al. published a study of glycosylate peptide nanosheets capable of sensing lectins (Con A and wheat germ agglutinin (WGA)) and Shiga toxin type 1 B subunit (Stx1B), through multivalent interactions.^[38] Peptides have been implemented to optimize the performance of these sensors; they are N-substituted glycine residues in which the side chains are attached to the nitrogen of the main chain.^[39] The use of peptides has the advantage of enhancing the control of the monomer sequence and “imitate” the cell membrane through their self-assembly in the form of nanosheet. The nanosheet is functionalized through glycosylation reactions through different peptides (Figure 2A). Particularly, these corresponded to mannose and N-acetylglucosamine, both targeting Con A and WGA. Two routes were followed: the first consisted of the glycosylation of the free peptoid followed by the self-assembly into functionalized nanosheets. The second route consists of nanosheets, which are first formed with the alkynylated peptoid, followed by

a sugar conjugation. For the detection of Con A, the optimum device consisted of a mixture of two peptoids with a mannose functionalization and a spacing of no more than 3 nm between its units. For the detection of WGA, two peptides were also incorporated with a separation distance of 1.2 nm between the units of *N*-acetylglucosamine. The scope of this study is the demonstration of the surface engineering of peptoid nanosheets that mimic some of the properties of the cell membrane, which interact with multivalent proteins. So far, these devices still lack the accuracy and selectivity demanded in real-world applications, but new approaches continue emerging to improve their performance.

More recent studies have integrated nanosheets into surface tension immunosensors.^[40] Immunosensors are a type of biosensor that combines a biological recognition mechanism with a transducer. The working principle relies on the molecular recognition between antigens and antibodies to form a stable complex.^[41] Then, a measurable signal in response to changes in the concentration of a given biomolecule.^[42] Here, the immunosensor was integrated with a micro-electromechanical system (MEMS) through an optical interferometer. The microcavity is then sealed by transferring a nanosheet of parylene C with low gas permeability.^[40] The nanosheet created from polymethyl methacrylate (PMMA) and parylene C is used as a “deformable membrane” on a silicon substrate with a microcavity structure. This device is capable of detecting human serum albumin (HSA). HSA constitutes 60% of total plasma protein^[43] and is employed as a valuable biomarker of many diseases, such as cancer, rheumatoid arthritis, ischemia, post-menopausal obesity, severe acute graft-versus-host disease, and diseases that require monitoring of glycemic control.^[44] The detection of protein-based antigens is carried out through a modification in the nanosheet, through a process of chemical modification, where an antibody is bound to the PMMA. The binding of antigens to antibodies induces repulsion forces that deform the nanostructure of the nanosheet producing deflections on the freestanding membrane. These deflections induce a shift toward the longer-wavelength regime of the spectrum (Figure 2B). The creation of the sensor was developed in three steps: the first consisting of the creation of nanosheets of parylene-C on a substrate of silicon linked to a PMMA nanosheet; the second consisting of a photolithographic technique for the creation of microcavities in a substrate of silicon; and the third consisting of the fixation of the nanosheet of parylene-C. Through this process, the two nanosheets of parylene-C (developed separately) were finally fixated. For the detection of the antigen, an oxidation process was developed in the PMMA sheet to form carboxylic terminal groups. Furthermore, the PMMA was activated for 30 min using 1-ethyl-3-(3-dimethylaminopropyl) carbodiimide (EDC)/*N*-hydroxy succinimide (NHS) to immobilize the antibody (anti-HAS) on the surface as a cross-linking agent. Finally, the developed sensor showed high sensitivity, with a detection limit of 0.1–1 fg mL^{−1} for HSA.

More recently, terahertz (THz) biosensors have also been integrated for protein detection, most of these with the addition of nanoparticles.^[45–49] Terahertz biosensors utilize the principle of resonance in the submillimeter wavelength regime. However, this mechanism has also been expanded to the gigahertz (GHz) regime.^[50] Each molecule analyzed through THz spectroscopy contains a characteristic “fingerprint,” which allows its analy-

sis and detection through specific biosensors for each molecule. Zhou et al. described new terahertz biosensors,^[51,52] which have greater specificity in the detection of multiple types of molecules. These sensors are nanostructured materials, also known as metamaterials, containing hydrated hydrogels functionalized with aptamers. Aptamer hydrogels are 3D hydrophilic and insoluble polymeric networks that are grafted by hydrated aptamers. The metamaterial was manufactured with a standard photolithography technique (with Cr/Au metal evaporation) and activated with oxygen plasma to improve hydrogel adhesion. The hydrogel was synthesized with aptamers (S1: 5'-acrydite-TTT AGT CCG TGG TAG GGC AGG TTG GGG TGA CT-3') and (S2: 5'-acrydite-TTT TTT CCA ACC TGC CCT GG-3'), with a precursor solution of acrylamide (Am), *N,N*-methylene-bis-acrylamide (MBAA), and ammonium persulfate. This sensor was capable of detecting the protein α -thrombin (h-TB). The α -thrombin is a trypsin-like glycosylated serine proteinase generated at the penultimate step of the blood coagulation cascade process from the circulating plasma protein prothrombin.^[53] Thrombin plays a central role in the initiation and spread of multiple events related to thrombotic vascular diseases, being one of the leading causes of mortality in the industrialized world.^[53] The attenuated total reflection is measured through spectroscopic methods for high-absorption liquids in the THz range.^[54] To model this effect, a 3D finite-difference time-domain (FDTD) simulation method was utilized to observe the behavior of the biosensor in the THz regime. The simulations showed that the intensity of the resonance peak of the THz biosensors increased with the thickness of the hydrogel in the range of 0–10 μ m, with a gradual saturation for thicker films, reaching a maximum of 50 μ m. This effect originated due to the density of cross-linking, i.e., the number of physical and chemical cross-links present in the polymer network, and the thickness of the hydrogel, which are critical for sensitivity and response time.^[51]

In line with protein sensors, various investigations have been carried out based on nanopores. In contrast to hydrogels, nanopores are commonly fabricated from patterned synthetic materials such as inorganic or plastic membranes, or from channel proteins in lipid membranes.^[55] However, nanopores have presented various limitations; for example, although nanopores have good specificity for single types of molecules; proteins tend to translocate through the nanopore too quickly to be accurately measured (Figure 2C). Acharya et al. described a novel sensor capable of measuring the immunoglobulin G1 (IgG) protein with hydrogel-backed nanopores (but also tested with bovine serum albumin (BSA) and streptavidin).^[56] Here, the hydrogel at the distal side of the nanopore was interacting sterically with the translocation of native proteins to increase the response time within the nanopore. A polyethylene glycol–dimethacrylate (PEG–DMA) hydrogel with a pore size smaller than the analyte (\approx 3.1 and \approx 5–10 nm, respectively) was utilized. This work showed \approx 418 events s^{−1} (Hz) for the detection of IgG, compared to a nanopore sensor, which presents 0.49 Hz. Additionally, a 963 pA current blockade amplitude for the hydrodynamic diameter of the proteins (10.8 nm with a pH 10) was expected for the sensor with hydrogel, this value corresponds with the previously reported IgG.

The research in nanopores continues expanding and diversifying in terms of fabrication methods and applications. In 2018, a novel mechanism involving ion-conducting nanopores (iNAPO)

was proposed.^[43] This concept combined protein-based biological nanopores with polymer-based nanopores. Several steps were followed for the manufacture of nanopores in the polymer sheet (consisting of terephthalate polyethylene sheets and polycarbonate). The sheet was irradiated with energetic gold ions, produced through vaporization and ionization, followed by an acceleration in high-frequency electrostatic fields. The irradiated polymer sheet was placed in a solution of an alkaline attack reagent monitored through two electrodes. Once these showed current flow, it was assumed that nanopores (usually conical in shape) were already formed. The chemical etching of the polyester structure leaves a terminal carboxyl group on the surface of the nanopore due to hydrolysis of the present ester groups. These carboxylic groups were bound to amine groups through coupling reactions with EDC/pentafluorophenyl esters (PFP). The EDC/PFP reaction facilitates the incorporation of molecules such as mannose and enzymes, among others. The authors noted that the binding of biocompatible molecules is still in development. The authors propose that the biomolecules (e.g., streptavidin, lysozyme, etc.) to be analyzed reacted in a specific bioconjugation reaction with the receptor, and claim that the devices produced from biological sources also lead to changes in the shape of the nanopore, producing an open nanopore configuration. In this open configuration, the ions of the electrolyte can pass through, and the corresponding electric current can be measured (Figure 2D).

With the same principle of iNAPO, other alternative techniques for the detection of proteins in nanopores have recently been described. These include the incorporation of substrate-binding proteins (SBP) which can be linked with multiple ligands and increasing the reliability.^[57] SBP proteins, like substrate-binding domains (SBDs), form a class of proteins (as well as domains) that are usually associated with protein–membrane complexes for signal transport or transduction.^[58] These are composed of two domains (α and β) connected by a “flexible hinge” region. Generally, the binding ligand site is located between the two domains; in the absence of a ligand, an open cavity is formed between them, and in the presence of a ligand, this closes with the ligand in the cavity.^[58] Their main function is binding to substrates, although they also stimulate different signaling proteins (including chemoreceptors, sensor kinases, diguanylate cyclases/phosphodiesterases, and Ser/Thr kinases) which elicits a wide range of responses.^[59] Recently, a hybrid electric nanosensor comprising the use of these bacterial SBP proteins was designed to bound to a solid-state nanopore that enables phosphonate detection.^[60] The phosphonate-binding protein (PhnD), which was bound to (P(N,N-dimethylacrylamide (DMAA)-co-N-methacryloxysuccinimide (NMAAS)) polymers through –NHS bonds, was introduced into a poly(ethylene terephthalate) (PET) nanopore. This design resulted in a nanopore device, whose stream was dependent on both: the concentration of proteins and the ligand interactions with the protein (Figure 2E). The fabricated device was sensitive to 2-aminoethylphosphonate (2AEP or ciliatin), of which its structural fragments are typically found as conjugates of glucans, lipids, and proteins.^[61] For 2AEP, different pore sizes were utilized (148, 197, 220, and 340 nm) with a maximum detected current of 3.3 ± 0.8 nA. This sensor demonstrated a lower detection limit by a factor of 10^2 – 10^3 compared to other classical analytical methods.

3. Carbohydrate (Saccharides) Detection

The carbohydrate analyte discussed herein is referred to within the biochemical context, which in a broader context is better referred to as saccharides. Carbohydrates are some of the most abundant chemicals in the biological world.^[62] They provide the largest source of metabolic energy for most organisms and are important structural components in many cells. They have also other fundamental roles in organisms, including cellular communication, inflammatory processes, and the development of infections and diseases.^[63]

Carbohydrates have several types of interactions such as carbohydrate–carbohydrate or carbohydrate–protein. Carbohydrate–carbohydrate interactions are regarded as weak; however, the combination of multiple sites could produce a reasonably strong binding affinity producing effects in cell recognition and adhesion.^[63,64] On the other hand, carbohydrate–protein interactions are correlated with infections, inflammation, and cell adhesion.

In recent years, the creation and design of sensors for the detection of carbohydrates have boomed, particularly in the detection of glucose.^[65–72] Glucose is the most important substrate of cellular metabolism because it is the main source of energy for all species.^[73] In fact, every living cell requires glucose for survival. In humans, various parts of the body, such as the nervous system or blood cells, rely entirely on glucose as an energy provider.^[74] There are several diseases associated with glucose, but diabetes mellitus is by far the most deadly. It is estimated that 11.3% of deaths globally are associated with this disease, with almost half of them corresponding to young adults (below 60 years).^[75] Diabetes mellitus is a chronic disease characterized by chronic hyperglycemia resulting from defects in insulin secretion, insulin action, or both, and, as a result, it affects the glucose equilibrium in the body.^[76] One of the main reactions used for glucose detection corresponds to glucose oxidase (GOx) which catalyzes the oxidation of β -D-glucose to δ -gluconolactone through a two-step reaction.^[77] In the first part of the reaction, the β -D-glucose is oxidized to δ -gluconolactone by the cofactor of glucose oxidase, flavin adenine dinucleotide (FAD), which in turn is reduced to FADH₂. Subsequently, oxygen is reduced to hydrogen peroxide and FADH₂ is oxidized back to FAD.^[77] Sensor design has focused primarily on sensing through blood samples; however, fewer designs have focused on sensing by other means (e.g., urine, tears, or interstitial fluids).

Elsherif et al. demonstrated an optical glucose sensor based on a diffuser architecture in contact lenses through a micro-printing method that creates densely packed concavities in hydrogel films functionalized with phenylboronic acid.^[65] Phenylboronic acid derivatives have been employed as an alternative to enzymes to develop sugar-sensitive systems based on UV-visible absorption, fluorescence, circular dichroism, and surface plasmon resonance.^[78] The incorporation of phenylboronic acids in hydrogels in conjunction with the glucose-binding process induces the Donnan osmotic pressure resulting in volumetric changes in the matrix. Hydrogel functionalized with phenylboronic acid is a system that responds to glucose due to its affinity for the diol-containing molecule (Figure 3A). The structure of the diffuser was based on lens matrices that exhibited focal length

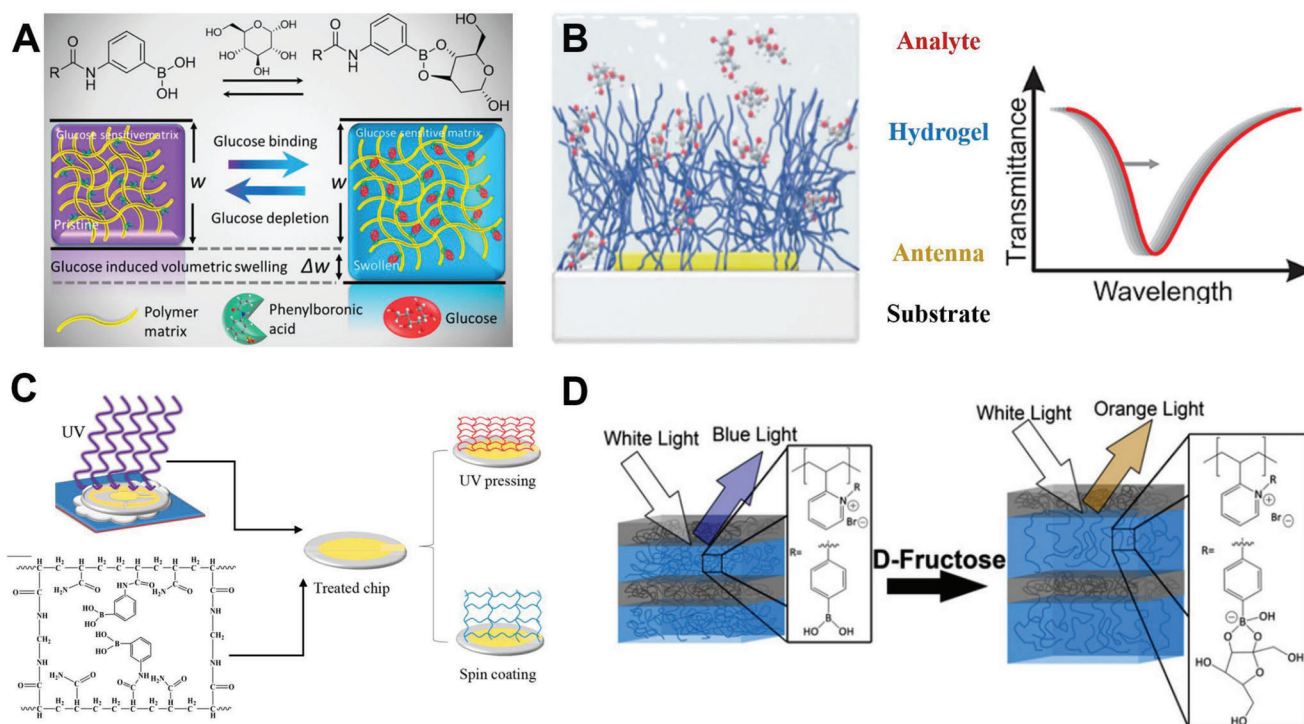


Figure 3. Techniques utilized for carbohydrate detection. A) Hydrogel matrix functionalized with phenylboronic acid and growth in the presence of glucose. Reproduced with permission.^[65] Copyright 2018, American Chemical Society. A microprinting method was utilized to create densely packed concavities in hydrogel films functionalized with phenylboronic acid. B) Hydrogel with plasmonic nanoantennas functionalized to produce a resonance displacement. Reproduced with permission.^[71] Copyright 2015, American Chemical Society. As the hydrogel swells, the ratio of polymer to water in the gel changes, and thus, the effective refractive index produces a redshift. C) Polymerization of the hydrogel through UV light followed by treatment. Reproduced with permission.^[72] Copyright 2020, American Chemical Society. This method showed changes in resonant frequencies in the presence of glucose. D) A 1D photonic crystal created from self-assembled lamellar blocks of copolymer. Reproduced with permission.^[92] Copyright 2013, Elsevier. The polymer film swells and expands due to the increase of negative charges on the P2PV.

modulation in response to modification of the overall hydrogel size following exposure to different glucose concentrations. The changing focal lengths, due to glucose concentration, changed the percentage of diffused light that is transmitted or reflected from the sensor surface, thus changing the light intensity of the diffuse point within a given transmission area. Concentrations of $0 \leq m \leq 100$ mM glucose were studied, showing higher sensitivity at pH 8. In the same way, other approaches have been considered for glucose detection in contact lenses. For example, Deng et al. have developed fluorescent contact lenses for monitoring glucose via smartphones.^[79] They used 2-hydroxyethyl methacrylate (HEMA) as the hydrogel network for the lens. Then by gelation of 6-aminohexyl methacrylamide (MAHA) and rhodamine fluorophore (RDMA), NHS active glucose probe (GS-NHS) was grafted in the hydrogel network. On one hand, HEMA was utilized to increase the mobility of the fluorescence probe and as an active amino site, and, on the other hand, RDMA was utilized as a fluorescent reference probe. Then, by fluorescent emission spectral measurement, the glucose properties were obtained, reaching a detection limit for glucose of $9.3 \mu\text{M}$, and a response time of over 3–5 s. When using a smartphone to read out the glucose concentration, the detection limit was $23 \mu\text{M}$, a value that meets the demand for tear glucose detection.

The development of polymer-based sensors has become an alternative to other noninvasive glucose monitoring. A novel

method proposed by Mesch et al. makes use of plasmonic nanoantennas connected to a hydrogel matrix. This sensor is based on gold nanoantennas, with plasmonic resonances in the near-infrared, placed on a glass substrate.^[71] These nanoantennas were covered with a thin layer of hydrogel and then developed from a monomeric solution of HEMA, ethylene glycol dimethacrylate (EGDM or EDMA), *N*-3-acrylamide phenylboronic acid (AAPBA). In this solution, the AAPBA was utilized to incorporate the sensing moieties within the hydrogel polymer. The phenylboronic acid forms a negatively charged complex with 1,2-*cis*-diols, such as glucose, which subsequently leads to an influx of water into the hydrogel, producing swelling. As the hydrogel swells, the ratio of polymer to water in the gel changes, and thus, the effective refractive index of the gel changes (Figure 3B). For glucose detection, the change in the effective refractive index of the hydrogel was monitored through spectral changes in the plasmonic resonance. Through this methodology, it was possible to reach a detection limit of 0.05 mmol L^{-1} of glucose. Furthermore, it was found that these results were independent of protein concentration since the hydrogel prevents macromolecules from entering the sensitive area around the gold antennas.

Another novel method designed for glucose detection includes quartz crystal microbalance (QCM) sensors. This type of sensor measures the mass of a material deposited on the surface of a quartz crystal as a function of the change in

the resonance frequency of the oscillating crystal.^[80] Recently, Dou et al. used the QCM principle for glucose detection with the addition of a poly(boric acid) hydrogel.^[72] A hydrogel-coated QCM electrode (fabricated from polyacrylamide (PAM)-3-(acrylamido)phenylboronic acid (3-APB) is utilized as a film with high specific adsorption. For the creation of this, a quartz “dish” was designed, and then a prepolymerized solution was deposited on a substrate, followed by the placement of the QCM electrode. Later, the QCM electrode was exposed to UV light for a full polymerization process (Figure 3C). The QCM electrode coated with the hydrogel had an improved detection limit (with 3 mg L⁻¹) compared to other techniques such as spin coating (detection limit of 100 mg L⁻¹), which was also studied in the same article. This type of sensor showed a detection range from 0 to 160 mg L⁻¹ with a pH in the range of 6.8–7.5.

In addition to glucose, sensors have also been designed for fructose detection. Fructose is a monosaccharide similar to glucose. However, it has been shown that excessive intake leads to various metabolic diseases such as insulin resistance, hypertension, and obesity among others.^[81] Recent studies have shown other complications associated with the high intake of fructose, which includes a high increment of postprandial hepatic de novo lipogenesis (DNL), triglycerides, and carbohydrate oxidation; a moderate increment in liver fat; and a dull suppression of endogenous glucose production (EGP) by insulin.^[82]

For the detection of fructose, techniques such as molecular printing (MIP) polymers have been performed. In this technique, a target molecule (or a derivative thereof) acts as a template where the interacting monomer is arranged and polymerized. These acquire a network or mesh shape to form a cast-like shell.^[83] Rajkumar et al. have studied the use of two different cross-linkers for fructose detection with this MIP technique and a flow calorimeter as a transducer.^[84] Wuff's covalent polymerization, which is a type of free radical polymerization, was utilized in this process.^[85] To prepare the fructose-imprinted polymer (MIP(Frc)), 2,2-azobisisobutyronitrile (AIBN) was added to two cross-linkers. The cross-linkers tested were β -D-fructopyranose 2,3,4,5-bis-O-((4-vinylphenyl) boronate), trimethylolpropane trimethacrylate (TRIM), or EDMA. In addition to the control MIP, with pinacol as a template and fructosyl valine MIP (MIP(Fru-Val)) 4-vinylphenyl, boronate esters were also added. Group binding studies were conducted to demonstrate the increase in the number of fructose molecules of MIP (frc) (reaching several nmols mg⁻¹ in time lapses of hours). In these trials, the cross-linker with the best performance was found to be TRIM. In equilibrium, TRIM-bonded MIP(Frc) binds to fructose 3.6 times more efficiently than the control polymer, and 1.4 times more than the MIP (Frc-Val). An injection of fructose for sensing leads to the formation of reversible covalent bonds with boronic acids within the microcavities of the MIP (Frc). The fructose polymer has been integrated into a thermistor for label-free online detection of fructose in the range of 0.5–10 mM.

Also self-assembled block copolymer (BCP) photonic crystals have been described for the detection of fructose. Self-assembled block copolymers have been widely used for self-assembled periodic structures derived from different polymer chains.^[86] Their application has been implemented in multiple configurations including 1D,^[87,88] 2D,^[89,90] and 3D^[91] photonic crystals. An interesting example is the sensor developed by

Ayyub et al. via the utilization of BCP. Here, they demonstrated a 1D photonic crystal created from a self-assembled lamellar block copolymer.^[92] The methodology consisted of a glass slide functionalized with 3-(aminopropyl) triethoxysilane (APTES), on which a solution (5% w/v) of polystyrene-*b*-poly block copolymer (2-vinylpyridine)(PS-*b*-P2VP) in propylene glycol monomethyl ether acetate was solidified using the spin-casting technique. To functionalize the block copolymer in a ratio of 0.95:0.05, the chemicals 2-(bromomethyl)phenylboronic acid (BMPBA) and 1,4-dibromo-2-butanol were utilized. Here, BMPBA acts as a functional group to bind sugar molecules, while the 1,4-dibromo-2-butanol acts as a cross-linker. The sensor functionality is dependent upon the formation of high-density negative charges on the boronic-acid-modified P2VP. Boronic acid is a Lewis acid; therefore, it can generate protons by abstracting a hydroxide unit from water. Through this process, both the proton and a negatively charged boronate anion are produced. These charges initiate the swelling, and hence, a change in the optical response of the polymer film is observed. Additionally, diols such as fructose bind to boronic acid. This process reduces the acidity and increases the amount of negatively charged units on the P2VP (Figure 3D). The results for D-fructose showed detectable concentrations in the range from 500 μ M to 50 mM. The detection limit under Phosphate-buffered saline (PBS) buffer conditions was 1 mM in these studies. In addition, the sensor showed high selectivity for fructose, even when it was mixed with other sugars such as glucose and sucrose. For instance, sucrose (which is a disaccharide) is much bulkier than fructose (which is a monosaccharide). It should be highlighted that, in contrast to monosaccharides, disaccharides produce steric effects, making them unfavorable to bind to boronic acid.

Fructose can also be detected through enzymes, such as D-fructose dehydrogenase (FDH). D-fructose dehydrogenase (EC 1.1.99.11) was discovered more than 50 years ago^[93] and has allowed the implementation of sensors for fructose, due to its high sensitivity and selectivity. Generally, FDH is used as an enzymatic catalyst (from the outer surface of the cytoplasmic membrane of *Gluconobacter* species) in the process of oxidation of D-fructose to 5-keto-D-fructose.^[94]

4. Ion Detection

Ions are essential in most biological reactions. For instance, metal ions stabilize, destabilize, or modulate biological molecules (i.e., proteins, enzymes, and nucleic acids) by introducing conformational changes and by creating centers of activity.^[95] Metal ions are required for normal cellular metabolism, but at higher concentrations, they can carry a health risk.^[96] Particularly, Ca²⁺, Mg²⁺, Zn²⁺, Cu²⁺, Fe²⁺, and Mn²⁺ are involved in multiple biological processes in the nucleus of cells through binding mechanisms with DNA and RNA. Their detection is expected in amounts of the order of 10⁻²–10⁻⁴ mol.^[97]

Different types of polymer-based sensors for the detection of ions have been reported in the literature.^[98–105] Recently, a solid-state cholesteric liquid crystal (CLC_{solid}) functionalized with an interpenetrated photonic polymer network (IPN) was demonstrated.^[99] Liquid crystals can combine properties such as anisotropic optical characteristics and molecular mobility.

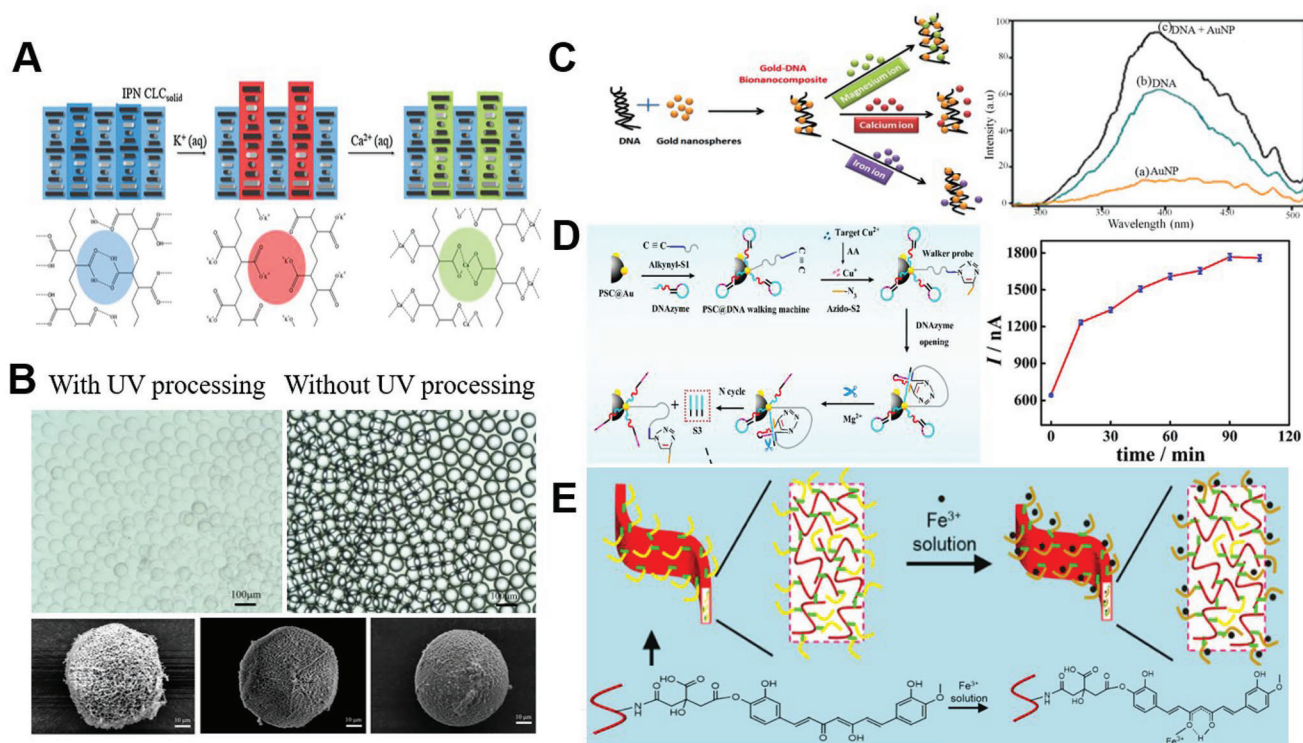


Figure 4. Chemical techniques used for ion detection. A) Solid-state cholesteric liquid crystal functionalized with an interpenetrated photonic polymer network. Reproduced with permission.^[99] Copyright 2019, Elsevier. A swelling process in the polymer film takes place due to the creation of COO—Ca—OOC bridges. B) Optical images of microdroplets with and without UV processing, in addition to SEM images (left to right) of PAA, PAAKOH, and PAAKOH—Ca X-droplets. Reproduced with permission.^[100] Copyright 2021, American Chemical Society. Here, a microfluidic method was used in an in situ process and then the droplets were functionalized with a KOH solution. C) DNA functionalized gold nanoparticles. Left panel: Interactions between Au—DNA nanocomposites and ions (Mg^{2+} , Ca^{2+} , and Fe^{3+}). Right panel: Fluorescence emission intensity observed from: AuNPs alone, DNA alone, and composite structures of AuNP—DNA. Reproduced with permission.^[110] Copyright 2017, the Authors. Published by Beilstein Institute. D) Click chemistry reaction to activate a 3D DNA walking machine. Left panel: Influence of the reaction time in click chemistry on the response observed in square wave voltammetry (SWV). Right panel: 3D walking machine activated by the chemical click reaction. Reproduced with permission.^[111] Copyright 2018, American Chemical Society. E) Diagram of the detection of ions with a solution of curcumin, citric acid, and zein with heating. Two solutions were utilized to create nanobelts with the electrospinning technique. Reproduced with permission.^[104] Copyright 2019, American Chemical Society.

In particular, cholesteric liquid crystals possess intrinsic periodicity in the form of a helical supramolecular structure.^[106] In its cholesteric phase, linear isotropy, birefringence, and chirality are present at the supramolecular level.^[107] Myung et al. developed an IPN with an O_2 plasma treatment to develop active sites within glass surfaces. This was treated with trichloro(1*H*,1*H*,2*H*,2*H*-perfluorooctyl)silane (PFOTS) and 3-(trimethoxysilyl)propyl methacrylate (TMSPMA) bound with a gap of 6 μm .^[90] To create the CLC_{solid}, a solution of RMM727 (which is a mixture of reactive mesogen used for liquid crystals) and S-4-cyano-4'-(2-methylbutyl)biphenyl (CB15) is placed in the gap of two glass surfaces, and then cured with UV. The two glass surfaces are correlated to a coating of PFOTS and TMSPMA, respectively. Another solution of AAC, tri(propylene glycol) diacrylate (TPGDA), and Irgacure 500 was placed on the sample. Functionalization was carried out with acetone and KOH to form a carboxylate salt. The creation of carboxylate salts allowed a metallic bond with divalent ions between the two carboxylate groups (COO— M^{2+} —OOC). It was shown that, in the treatment with acetone (without KOH), the water absorption accelerated, allowing sensitive pH changes between blue, green, and red colors (Figure

4A). In the case of the Ca^{2+} ion, it was found that an aliquot of 3.2 μL was enough to induce color changes in the sensor. The detection limit in this sensor was in the range of 0.4–3.5 mM.

Following the same principle of carboxylate salts, Hao et al. proposed monodispersed cross-linked poly(acrylic acid) (PAA) droplets (PAA X-droplets). Here, small spherical sensors of about 60 μm in diameter detected simultaneously Ca^{2+} and Mg^{2+} in saliva and serum.^[100] The mechanism in which ions are detected is through the formation of COO— M —OOC bridges. The PAA is chosen due to the capability of the carboxylic group to coordinate and bind divalent ions. This binding can be correlated with the amount of ion present in the sample through the swelling in the hydrogel. The sensor was developed using a polymicrofluidic(dimethylsiloxane) (PDMS) chip, which was designed to discharge aqueous solutions into the droplet storage chamber through the outlet. The polymerization solution included reagents such as acrylamide (AAm) and *N*'-methylenebisacrylamide (MBA) as the cross-linker. For the creation of the hydrogel droplets, the microfluidic method was applied with UV polymerization in an in situ process (Figure 4B). Subsequently, the droplets were functionalized with a KOH solu-

tion to maximize their response. This process occurs with the blocking of hydrogen bonds (HBs) between carboxylic groups through the complex formation of $\text{COO}^- \text{K}^+$. The sensor showed a response time of 10 min with a concentration of $113\text{--}86\text{ }\mu\text{M}$ of a solution of CaCl_2 10 mmol L^{-1} . High reversibility was achieved with droplets maintaining the original diameter of the drop ($113\text{ }\mu\text{m}$) with an HNO_3 treatment. However, at lower concentrations, the sensor needs more time to reach a contraction to smaller diameters. In this work, the droplets were functionalized for the detection of Ca^{2+} and Mg^{2+} in saliva and serum. The advantages of working on this configuration are its reusability, cost-effectiveness, and high accuracy.

Generally, sensors that detect Ca^{2+} ions also detect Mg^{2+} ions, which are the two main metal ions present in human serum. Both ions compete for the binding sites of divalent cations in DNA and RNA.^[108] It is known that the exchange of $\text{Ca}^{2+}/\text{Mg}^{2+}$ is vital for Ca^{2+} -regulated muscle contraction^[99] and that Mg^{2+} promotes Ca^{2+} entry into various tissues (this process is known as $\text{Ca}^{2+}/\text{Mg}^{2+}$ exchange).^[109] Sensors for Mg^{2+} detection have been developed with the aid of Au–DNA nanocomposites (NCs).^[110] For this, a small amount of mercaptopropionic acid (MPA) was added to the Herring sperm DNA (this was incubated in a laminar hood to ensure the binding of the alkanethiol to the oligonucleotides). MPA supports the stabilization, but also the functionalization, thanks to the affinity of the sulfur groups of thiol and gold. Also, DL-dithiothreitol (DTT) solution was added and incubated to cleave the disulfide bonds formed by the oligonucleotides upon the addition of MPA. DNA-functionalized gold nanoparticles (AuNPs) were then washed twice by centrifugation to remove all unbound alkanethiol double-stranded DNA. Due to the size- and shape-dependent plasmonic interactions of AuNPs (in the range of $33\text{--}78\text{ nm}$) with DNA, the resultant Au–DNA NCs exhibited superior fluorescence emission (Figure 4C). This effect was observed due to the chemical binding with Ca^{2+} , Fe^{2+} , and Mg^{2+} ions. Nevertheless, the system also showed selective detection of Mg^{2+} in a mixture containing Ca^{2+} , Fe^{2+} , and Mg^{2+} . The selectivity toward Mg^{2+} in the mixture can be attributed to the smaller size of Mg^{2+} , which supports the ionic linkage. In this sensor, a detection range from 20 to 800 ppm for Mg^{2+} ions was achieved.

To date, the use of electrochemical techniques has been one of the most successful methods for the detection of ions. This technique has not only been developed for Ca^{2+} and Mg^{2+} ions, but also for Cu^{2+} ions. Qing et al. developed a click chemistry reaction to activate a 3D DNA walking machine for ultrasensitive electrochemical detection of copper (Cu^{2+}).^[111] A DNA walking machine is understood as a unique class of dynamic DNA devices that move procedurally and autonomously along various tracks.^[112] The composition of the machine consisted of azido-labeled S2 (azido-S2) and alkynyl-labeled S1 (alkynyl-S1) (both different oligonucleotide sequences), and also a hairpin-locked deoxyribozyme (DNAzyme) assembled into aminated magnetic polystyrene microspheres with gold nanoparticles (PSC@Au nanocomposites) (Figure 4D). To prevent the formation of disulfides, all oligonucleotides modified with thiols were preincubated with a solution of Tris(2-carboxyethyl)phosphine hydrochloride (TCEP). In order to maximize the amount of oligonucleotide load, a NaCl solution was added. This process occurs because the DNA load can be increased by salt ageing.^[113] For

the manufacturing of the electrochemical biosensor, a glass carbon electrode (GCE) coated with AuNPs by electrodeposition was utilized. Here, the sites of nonspecific binding of the electrode were blocked with mercaptohexanol (MCH). Subsequently, a ligation of alkyl-S1 with azido-S2 was carried out, with the support of Azido-S2, Cu^{2+} , and sodium ascorbate (AA). The binding of alkyl and azido-DNA does not take place without the presence of the copper ion. However, when the Cu^{2+} ion is added, there is a reduction to Cu^+ with the help of AA. After the reduction takes place, there is a union of the alkyl and azido-DNA, generating a walker probe on the PSC@Au. Also, Mg^{2+} was added as a cofactor to provide activation of the DNAzyme, and hence to cleave the self-strand at the site of the ribonucleotide. This was accompanied by the release of the DNA product (S3), which was separated from the solution. The proposed biosensor was studied by square wave voltammetry (SWV) in the presence of Cu^{2+} (100 nM) in time intervals of 15 min (0, 15, 30, 45, 60, 75, 90, 105 min). It was observed that 90 min was the minimum time to reach the click chemistry. Also, it was shown that, without the presence of the Mg^{2+} cofactor, there was no binding of alkyl and azido-DNA in the DNAzyme, or was the product S3 generated. A detection range from 1 pM to 500 nM (with a detection limit of 0.33 pM) was determined. This strategy showed enhanced sensitivity and a wider linear range compared to other methods.

Other configurations such as polymer membranes in the form of nanobelts have also been described in the literature.^[114] Nanobelts are quasi-1D structurally controlled nanomaterials with characteristics such as well-defined chemical composition, crystallographic structure, and surfaces;^[115] usually, the basis of this type of nanomaterial is the electrospinning technique, which has been widely used for the detection of metal ions (e.g., Pb^{2+}). This technique consists of an electrodynamic mechanism capable of extracting continuous fibers from an injected polymer solution.

Qiao et al. also utilized the electrospinning technique to create a sensor for the detection of Fe^{3+} .^[104] Fe^{3+} plays a key role in many biochemical processes at the cellular level and is indispensable for most organisms. In addition to providing the oxygen transport of heme, it also acts as a cofactor in many enzymatic reactions involved in the mitochondrial respiratory chain. However, high levels of Fe^{3+} in the human body are correlated to organ dysfunction and a higher incidence of cancer.^[98] To create nanobelts, a solution of zein, citric acid, and curcumin was mixed with an ethanol solution. Citric acid acted as the cross-linker, while curcumin was used as a chelating agent in the detection of the metal ion (Figure 4E). Two solutions of zein, citric acid, and curcumin at $1:0.09:0.05$ mass ratio were utilized, one without undergoing a process of heating and the other with heating (2.5 h at $150\text{ }^\circ\text{C}$). Both solutions were utilized to create the nanobelts with the electrospinning technique ($15\text{--}18\text{ kV}$, 0.9 mL h^{-1}). Then, the electrospun nanobelt-shaped membranes were placed in contact with a solution of Fe^{3+} . After analysis by scanning electron microscopy (SEM), both membranes (unheated and heated) showed a contraction after contact with the Fe^{3+} of $8\text{--}4.7$ and $8\text{--}6.5\text{ mm}$, respectively. This effect demonstrated that nanofibers/nanobelts would interblend after water immersion. Detection limits of 1 and 0.3 mg L^{-1} were observed for the unheated and heated nanobelt-shaped membranes. In turn, with the support of Attenuated Total Reflectance-Fourier Transform

Infrared (ATR-FTIR) spectroscopy, it was found that the ion can bind the curcumin, confirming that it is possible to apply a chelating agent for the detection of Fe^{3+} . Curcumin contains two possible sites to bind with the ion, the phenolic hydroxyl group and the functional group β -diketo. It was concluded that during the ion detection process, a cavity β -diketo is formed with the support of a bond between eno-enol hydrogen.

According to the reported literature, the detection of ions also focuses on environmental monitoring, where the detection of heavy metals is of utmost importance. Given the consequences that pollution can have on drinking water or agriculture, special attention has been placed on the use of functionalized nanoparticles containing capping agents (surfactants and ligands), which can enhance the bioactivity of nanoparticles and protect them from the environment.^[108,116–118] Other techniques such as composites^[119] with electrochemical have also been implemented.

5. DNA Detection

DNA is a molecule that contains all the information of an organism to self-replicate and self-maintain. DNA is composed of thousands of nucleotides, which are formed by a sugar molecule, which binds to a phosphate group and a nitrogenous base. The nitrogenous bases found in DNA are adenine (A), cytosine (C), guanine (G), and thymine (T).^[120] The methods to detect and quantify DNA have increased steeply since its discovery.^[121] Various techniques involving polymers have been described for the recognition of nucleotides, most of them, with the application of nanopores.^[122–127] Nanopores are capable of detecting nucleotides through cavities, which are fabricated through self-assembly, origami, and solid-state, among others. The DNA origami technique has been widely utilized since it was first proposed by Seeman.^[128] In this work, Seeman showed the assembly of DNA nanostructures with precisely controlled features and geometries. Furthermore, an assembly of complex and multidimensional objects were generated through the pairing of adhesive end bases from individual structures. In the origami technique, DNA is folded to create 2D and 3D objects at the nanoscale producing a long single-stranded scaffold DNA (ssDNA) annealed with multiple short staples (hundreds of designed short ssDNAs). The staples can bring together distant regions of the scaffold via base pairing, resulting in a prescribed shape.^[129]

Through DNA origami and nanopores, Farimani et al. developed a hybrid graphene nanopore for DNA detection in a computer-simulated environment.^[130] This nanopore device was functionalized with “hanging” unpaired T bases (Figure 5A). The developed sensor had a pore size of 2.1 nm and a graphene sheet of 10 nm × 10 nm. For the development of DNA origami, a caDNA software was implemented. A double layer of DNA origami was simulated for comparison. For functionalization, the origami structure was modified in the graphene pore part by removing eight A bases from the “staple” filament and leaving eight unpaired T bases in the “scaffold filament”. The use of T bases in the pore can induce specific interactions with DNA capable of translocating mostly with its complementary base A. DNA detection occurs through the interaction of “specific signatures” that usually reduce the speed of translocation of ssDNA. Several simulations were performed with different configurations including

a bare graphene nanopore, a single-layer DNA origami hybrid nanopore and a double-layer DNA origami hybrid nanopore. The highest conductance value was for the graphene sheet, while the lowest was for the double-layer DNA origami hybrid nanopore. Also, simulations were performed to investigate the speed of translocation of ssDNA poly(dA)₂₀, poly(dC)₂₀, poly(dG)₂₀, and poly(dT)₂₀. The fastest transition rate was observed for the hybrid DNA origami nanopore of a poly(dG)₂₀ layer followed by poly(dC)₂₀ and poly(dT)₂₀ (poly(dA)₂₀ which presented the slowest translocation. Only 15 bases were successfully translocated and the last five bases were glued into the pore for more than 30 ns. Here, 20 simulations were performed to find the statistical distribution of dwell times. In the case of base A, a time of 2 ns was found, for base C a time of 1.6 ns, for base G a time of 0.75 ns and for base T a time of 0.64 ns. The average numbers of HB between the ssDNA and the nanopore region of the single-layer DNA origami of hybrid nanopore were also obtained (poly(dA) ≈ 0.95, poly(dG) ≈ 0.85, poly(dC) ≈ 0.85, and poly(dT) ≈ 0.3). Base A had the highest HB, while base T had almost no HB. Finally, functionalized DNA origami was found to be stable in the presence of thermal noise, ionic permeation, and water, and electrophoretic translocation of DNA.

Other materials used for DNA detection, such as hydrogels, have been used to a lesser extent.^[131–134] Sulaiman et al. developed a method with hydrogel-filled nanopores (HFN) that combine quartz nanopipettes with hydrogels developed from a UV copolymerization of biocompatible poly(vinyl) alcohol (PVA) (Figure 5B).^[131] The chemical properties of the hydrogel were controlled with acetylation of PVA to obtain certain functionalities. For instance, the cationic sample was developed through ammonium, the anionic sample through carboxylate groups, and the hydrophobic through phenyl groups. Moreover, the ion transport was studied for each of these samples; for those of negative charge (anionic carboxylate functional group (CO_2^-)), a strong rectification ratio of negative charge of 3.8 ± 1.4 (rectification ratio at ± 400 mV) was observed. For those of positive charge (cationic ammonium functional group (NH_3^+)) a considerably lower rectification of 1.2 ± 0.1 was observed. This difference occurs due to the positive charge on the hydrogel that neutralizes the walls of the negative pores. Further investigations of the effects of DNA transport conducted through translocation were studied with 250 bp double-stranded DNA (dsDNA). The results showed that concentrations of 15 wt% PVA- CO_2^- allowed the detection of DNA of 250 bp for carboxylate groups, while the translocations were measured as 10 and 15 wt% de PVA- NH_3^+ . Subsequently, both the sensitivity and efficiency of analyte detection were improved by modifying the mesh size of the hydrogel. The optimum value was found with an average mesh size of less than half the size of the analyte. Finally, a test was performed with a mixture of dsDNA fragments of 100 bp, 250 bp, and 10 kbp. It was found that the sensor developed with PVA-OH-HFN was able to detect the fragments of 100 and 250 bp, but not the sample with 10 kbp fragments.

DNA detection with colourimetric techniques through the use of hydrogels has also been proposed. Baeissa et al. developed functionalized monolithic hydrogels with DNA and AuNP for high-sensitivity colourimetric DNA detection.^[135] Here, a layer of polyacrylamide hydrogel created from a stock solution of gel (acrylamide/bisacrylamide), as well as sodium nitrate,

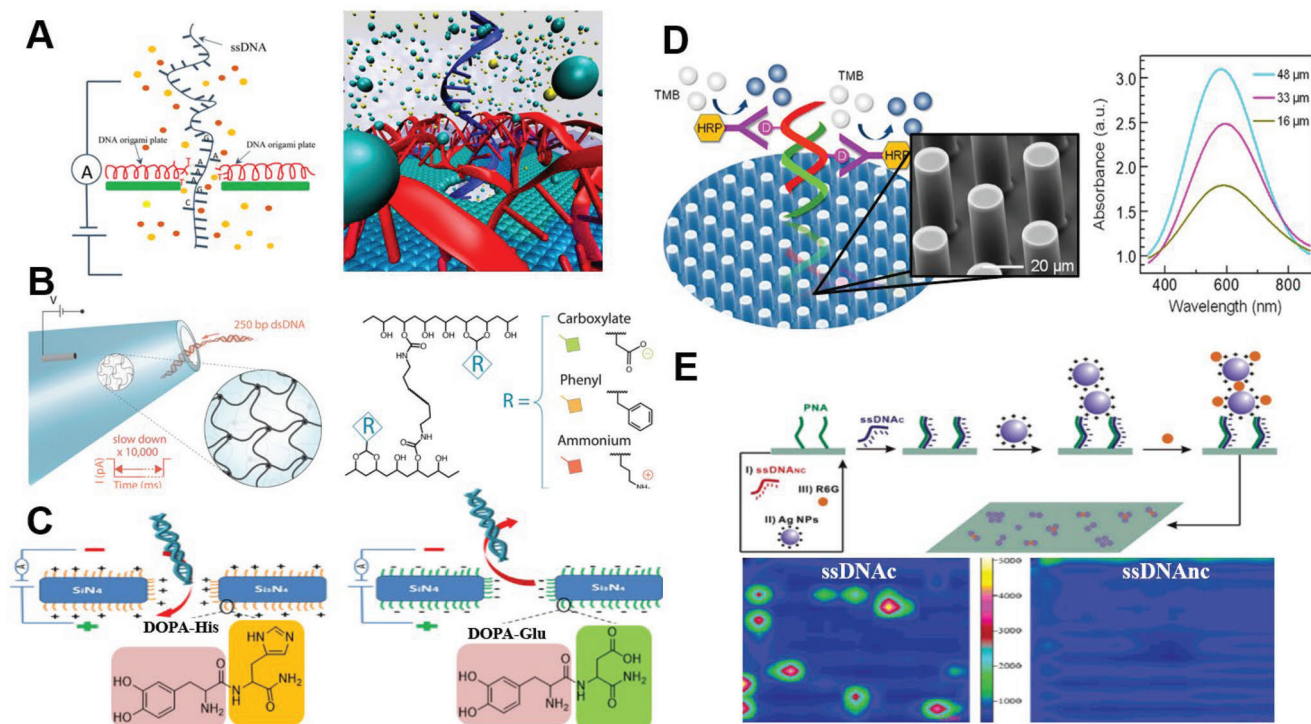


Figure 5. Chemical processes and techniques used for DNA detection. A) DNA origami and nanopores. Left panel: Representation of ion current showing the interaction of the complementary bases (A–T). Right panel: Illustration of a hybrid of graphene nanopore for DNA detection where a single-layer DNA origami is represented in red and translocated ssDNA in blue, also a sheet of graphene, water, and ions can be observed. Reproduced with permission.^[130] Copyright 2017, American Chemical Society. B) Hydrogel-filled nanopores (HFN). Left panel: HFN sensor's structure featuring a nanoporous mesh that is cross-linked at the tip of the nanopipette. Right panel: Chemical composition of photo-cross-linked PVA-based hydrogels, with three functional groups. Reproduced with permission.^[131] Copyright 2018, American Chemical Society. C) DNA recognition in various nanopores functionalized with DOPA–amino acids. DOPA functions as an anchor group to functionalize the pore with the various amino acids. Both, complementary and noncomplementary ssDNA were tested. Reproduced with permission.^[137] Copyright 2020, American Chemical Society. D) Implementation of polymer micropillar for colorimetric DNA detection. Left panel: Periodic matrices of micropillars produced from a cyclic olefin copolymer by high-fidelity micro-fabrication for colorimetric DNA detection. Right panel: Absorbances for various sizes of microcapillaries. Reproduced with permission.^[138] Copyright 2020, American Chemical Society. E) PNA-based SERS method for DNA detection and SERS maps obtained for ssDNAC and ssDNACnc corresponding to the integrated area of the R6G peak at 1648.5 cm^{-1} . Reproduced with permission.^[141] Copyright 2007, American Chemical Society.

Tris nitrate, acrydite DNA, and water was described. The DNA-functionalized AuNPs were presented with two sizes, 13 and 50 nm, both receiving specific treatments. For the experiment, the hydrogels were placed in a solution of AuNPs and the target DNA was tested at different concentrations. Here, the bounding of AuNPs caused color formation in the hydrogel from a clear aspect to red. Furthermore, AuNPs work as a catalyst for the reduction of silver ions to metallic silver, producing a black color in the hydrogel. The results showed low optical background and visual detection in the nanomolar regime ($\approx 0.1\text{ nM}$ of the target DNA) with DNA-functionalized AuNPs. In contrast to other frequently used surfaces for DNA immobilization, monolithic hydrogels can be shaped into arbitrary forms and handled similarly to homogeneous assays while still having reversibility and signal amplification.

The utilization of peptides is another common way to functionalization. These are described as the union of various amino acids by amine bonds, and unlike proteins, these have shorter polymer chains.^[136] Karmi et al. developed a coating of Si_3N_4 nanopore with several self-assembled dipeptide monolayers.^[137] Here, the amino acids' histidine, lysine, and glutamate were coated with

amino-L-3,4 dihydroxyphenylalanine (DOPA); DOPA functions as an anchor group to functionalize the pore with the various amino acids (Figure 5C). The nanopores were fabricated through the perforation on a SiN membrane with the aid of an electron beam. The membrane doped with L-3,4-dihydroxyphenylalanine (DOPA) residue (the anchoring element) was placed in a solution of each dipeptide (histidine, lysine, and glutamate). Subsequently, each functionalized pore was placed on a chip mounted in an electrophoresis flow cell. To obtain ion current measurements, a pair of Ag/AgCl electrodes were connected, and a double Faraday cage was utilized to avoid external electrostatic interference. The ion current results showed consistent readings for up to 7 months without any additional treatment. In the case of glutamic acid, it was observed that the pH is affected depending on the amino acid applied. For example, glutamic acid acquires a negative charge as soon as the pH increases, while for histidine a positive charge is obtained as soon as the pH decreases. The effect of pH on each amino acid load affects its Debye length: as the salt concentration (KCl) increases, the Debye length shortens. Also, the ionic current was measured for the sample with translocated dsDNA on the nanopores functionalized with DOPA–histidine

(DOPA-His). It was shown that for short DNA (2 kbp), there are faster dwell times (0.1 ms), while for long dsDNA (48 kbp) the times were 5 ms. For DOPA–Glu there was no change in conductance for a pH of 7.5 due to the repulsion of the DNA located above the pore. In the case of DOPA–Lys there were fluctuations between two arbitrary levels. Finally, Si_3N_4 nanopores coated with DOPA enabled a range of sensing applications (such as pH and salt detection) and control of the translocation time of analytes such as DNA.

The implementation of polymer micropillar arrays as templates for colourimetric DNA detection was recently reported.^[138] The polymer used in this study (Zeonor) was a thermoplastic cyclic olefin copolymer (COC). Zeonor was described as durable, chemically inert, nontoxic, and optically transparent in the visible and near-infrared regime.^[139] This polymer was configured in microcapillary matrices by hot stamping techniques with the aid of two master moulds. Both master moulds were prepared with a silicon sheet and a fluorinated ethylene–propylene (FEP) sheet. Micropillar array substrates were exposed to oxygen plasma, which activated structural and planar portions of the surface simultaneously. In addition, the substrates were treated with CNBr and acetonitrile. Oligonucleotide samples were moved onto the Zeonor substrate with slotted pins and then heated to complement the bonding process. Immobilizing oligonucleotide probes achieved through the formation of hydroxyl groups on the Zeonor surface with oxygen plasma treatment. The oligonucleotide probes were modified with amino in the 5' position together with an internal spacer of hexaethylene glycol, for both, on the top of the pillars and in between the pillars. Subsequent use of CNBr converted these groups into reactive cyanate ester groups. The hydrophilic nature of the activated substrate, coupled with the use of buffer solutions containing blocking agents, maintained the nonspecific adsorption of amplicon and antibody molecules at negligible levels. In turn, the coupling of the cyanate ester with a raw amine resulted in a stable derivative of isourea. For detection, solutions of amplicon, antibody, and 3,3',5,5'-tetramethylbenzidine (TMB) were utilized to induce coloration from clear to blue, which reveals the presence of the target gene. Furthermore, genetic markers amplified by polymerase chain reaction (PCR) for *Escherichia coli* O157:H7 (rfbO157, eae, vt1, and vt2) were included with the addition of a detectable digoxigenin label (Figure 5D). The presented results were not quantitative and only showed a “Yes,” in the blue cooler, or a “No” when there was no change of coloration. Further studies were also performed to correlate the distances in the microcapillary arrangements and the coloration effects.

Another novel technique for DNA detection is based on the use of SERS. SERS can be utilized for sensitive and selective molecular identification. In recent years it has been widely applied as a signal transduction mechanism in biological and chemical detection.^[140] Fabris et al. proposed a single-stranded DNA identification method (ssDNA)^[141] taking advantage of peptide nucleic acids (PNAs) bound to a surface. Here, electrostatic interactions that produce SERS signals after ssDNA/PNA hybridization are monitored (Figure 5E). One of the advantages of this method is that only one electrostatic deposition of metal clusters is needed, and no metal SERS substrate is required. For this method, the PNAs with a 5'-TCC ACG GCA TCT CA-3' sequence were printed on an isothiocyanate-activated glass slide.

Once complementary ssDNA (a DNA copy of a messenger RNA (mRNA) molecule produced by reverse transcriptase) was added, a surface with a net negative charge is formed. This process was also carried out with noncomplementary ssDNA. As a result, when positively charged silver nanoparticles (AgNPs) are added, a link is created. The slides with the AgNPs were immersed in a solution containing a suitable SERS reporter: Rhodamine 6G (R6G). This reporter is chosen because of its interaction with silver surfaces, the lack of charge repulsion with the NPs and its absorption maximum tunability with the laser wavelength (514.5 nm) for resonance enhancement. The results of the SERS signals were analyzed with the two types of ssDNA (complementary and noncomplementary), showing a clear difference between both types, being the complementary ssDNA the most favorable. The density of strongly scattering sites for complementary ssDNA was $\approx 0.007 \mu\text{m}^{-2}$. Also, the formation of aggregates of AgNPs was reported, creating 10% of the SERS signal. Later, these aggregates were analyzed by atomic force microscopy (AFM).

6. Conclusion

In this review, we have explored various types of polymeric biosensors categorized according to their target biomarkers. The review encompasses a wide array of methods wherein functionalized polymers have been successfully utilized for biomarker detection. To facilitate this exploration, this review classified the sensing methods according to the type of target analyte. The four main targets discussed in this review include proteins, carbohydrates, ions, and DNA. In the case of carbohydrates, the most utilized targets were glucose and fructose, which are correlated to multiple human diseases in the modern world. The techniques applied for carbohydrate detection include the use of terahertz sensors, MIPs, electrochemical sensors, and fluorescent colourimetric chemosensors, among others. For the detection of proteins, most of the sensors are based on the detection of viruses and lectins. Some of the most common functionalized polymers are PAAm, PAm, and to a lesser extent PEG. In the case of the detection of metal ions, the literature found was mostly based on environmental applications. However, within the biosensors applied in the human body, nanobelts have emerged as a promising configuration for the Fe^{3+} detection. Finally, for the detection of DNA, most of the sensors investigated rely on functionalized nanopores. Most of the research in DNA detection remains at the simulation level through computational algorithms capable of evaluating their viability.

Despite the impressive progress in the field, there are evident persistent challenges to be addressed. Among the primary challenges in the functionalization of polymers, the selectivity of the biomarkers is one of the main concerns for successful implementation. To date, several problems such as interference and cross-talk emerge in the presence of multiple analytes. Addressing this issue requires an exhaustive exploration of the underlying chemistry to identify suitable ligands that exhibit high specificity toward the biomarkers, along with careful consideration of the material and nanomaterial preparation mechanisms. High resolution and accuracy are also challenges to address in the context of polymeric biosensors. Leveraging nanomaterials hold promise in enhancing detection sensitivity, but it is essential to prioritize reproducibility and standardization to ensure reliable results across

different experiments and laboratories. Lastly, principal attention should be given to the biocompatibility of the materials used. To pave the way for potential integration with existing technologies, researchers must focus on developing nontoxic materials that can interact with biological systems, safeguarding both human health and the functionality of the integrated systems. By addressing these challenges, nanotechnology-based biomarker detection can open new possibilities in diagnostics and personalized biosensors.

Rounding up, the development of biosensors with functionalized polymers has emerged as a new approach in various applications involving pathology detection with the help of various nanomaterials and configurations; much lower detection limits are reached day to day. With the possibility of identifying diverse analytes, and in smaller amounts, not only the detection of a wider range of diseases is becoming attainable, but also new avenues in reversible, low-cost, and in situ monitoring are being opened. According to the publication rate of the past 5 years, a promising future for functionalized polymers can be forecasted. The use of polymers in sensors will be determinant in the coming decade, detonating research, innovation, and the development of new families of biosensors.

Acknowledgements

This project has received funding from the European Union's Horizon 2020 research and innovation programme under the Marie Skłodowska-Curie grant agreement No. 896410.

Conflict of Interest

The authors declare no conflict of interest.

Keywords

biomarkers, functionalization, polymers, sensors

Received: August 7, 2023

Published online: October 9, 2023

- [1] A. J. Jose, M. Alagar, in *Manufacturing of Nanocomposites with Engineering Plastics*, Woodhead Publishing, Cambridge, UK **2015**, pp. 31–59.
- [2] Y. C. Lu, J. H. Mao, W. Zhang, C. Wang, M. Cao, X. D. Wang, K. Y. Wang, X. H. Xiong, *Chemosphere* **2020**, 238, 124640.
- [3] M. Gaeta, M. Barcellona, R. Purrello, M. E. Fragalà, A. D'urso, *Chem. Eng. J.* **2022**, 433, 133262.
- [4] M. Catauro, M. C. Mozzati, F. Bollino, *Acta Astronaut.* **2015**, 117, 153.
- [5] M. Lv, Q. Wang, T. Wang, Y. Liang, *Composites, Part B* **2015**, 77, 215.
- [6] C. García, M. Fittipaldi, L. R. Grace, *J. Appl. Polym. Sci.* **2015**, 132, <https://doi.org/10.1002/app.42691>.
- [7] M. Zare, K. Namratha, S. Ilyas, A. Hezam, S. Mathur, K. Byrappa, *ACS Appl. Mater. Interfaces* **2019**, 11, 48309.
- [8] Y. Luo, Q. Wang, Y. Zhang, *J. Agric. Food Chem.* **2020**, 68, 12993.
- [9] Y. Hu, F. Liu, J. Pang, D. J. McClements, Z. Zhou, B. Li, Y. Li, *J. Agric. Food Chem.* **2021**, 69, 730.
- [10] L. Burratti, F. De Matteis, M. Casalboni, R. Francini, R. Pizzoferrato, P. Proposito, *Mater. Chem. Phys.* **2018**, 212, 274.
- [11] M. M. Thomas, P. R. Chandran, V. V. Vipin, A. P. Mohamed, P. Kingshott, S. Pillai, *React. Funct. Polym.* **2021**, 158, 104779.
- [12] C. Liu, C. Yao, Y. Zhu, J. Ren, L. Ge, *Sens. Actuators, B* **2015**, 220, 227.
- [13] Y. Li, L. Zhou, G. Liu, L. Chai, Q. Fan, J. Shao, *Appl. Surf. Sci.* **2018**, 444, 145.
- [14] F. Wang, Z. Zhu, M. Xue, F. Xue, Q. Wang, Z. Meng, W. Lu, W. Chen, F. Qi, Z. Yan, *Sens. Actuators, B* **2015**, 220, 222.
- [15] W. Lu, H. Li, B. Huo, Z. Meng, M. Xue, L. Qiu, S. Ma, Z. Yan, C. Piao, X. Ma, *Sens. Actuators, B* **2016**, 234, 527.
- [16] M. J. McGrath, C. N. Scanail, in *Sensor Technologies*, Apress, Berkeley, CA **2013**, pp. 15–50.
- [17] A. Michelmore, in *Thin Film Coatings for Biomaterials and Biomedical Applications*, Woodhead Publishing, Cambridge, UK **2016**, pp. 29–47.
- [18] R. Hu, T. Liu, X.-B. Zhang, S.-Y. Huan, C. Wu, T. Fu, W. Tan, *Anal. Chem.* **2014**, 86, 5009.
- [19] Y. Hu, X. Xu, Q. Liu, L. Wang, Z. Lin, G. Chen, *Anal. Chem.* **2014**, 86, 8785.
- [20] Z. Xu, Y. Chang, Y. Chai, H. Wang, R. Yuan, *Anal. Chem.* **2019**, 91, 4883.
- [21] Y. Li, R. Han, M. Chen, X. Yang, Y. Zhan, L. Wang, X. Luo, *Anal. Chem.* **2021**, 93, 14351.
- [22] G. J. Zhang, M. J. Huang, J. J. Ang, Q. Yao, Y. Ning, *Anal. Chem.* **2013**, 85, 4392.
- [23] M. Xu, Y. Zhu, S. Gao, Z. Zhang, Y. Gu, X. Liu, *ACS Appl. Nano Mater.* **2021**, 4, 12442.
- [24] R. Zou, S. Shan, L. Huang, Z. Chen, T. Lawson, M. Lin, L. Yan, Y. Liu, *ACS Biomater. Sci. Eng.* **2020**, 6, 673.
- [25] J. Hu, S. Liu, *Macromolecules* **2010**, 43, 8315.
- [26] B. V. Elsevier, *Scopus*, <https://www.scopus.com/home.uri> (accessed: November 2022).
- [27] Y. Tang, H. Wang, S. Liu, L. Pu, X. Hu, J. Ding, G. Xu, W. Xu, S. Xiang, Z. Yuan, *Colloids Surf., B* **2022**, 220, 112973.
- [28] Y. Zhu, P. Xu, X. Zhang, D. Wu, *Chem. Soc. Rev.* **2022**, 51, 1377.
- [29] A. Blanco, G. Blanco, in *Medical Biochemistry*, Elsevier, Amsterdam **2017**, pp. 21–71.
- [30] J. M. Berg, T. J. Tymoczko, L. Stryer, *Biochemistry* **1988**, 27, 8509.
- [31] M. W. Gonzalez, M. G. Kann, *PLoS Comput. Biol.* **2012**, 8, e1002819.
- [32] H. Wu, *J. Biol. Chem.* **1922**, 51, 33.
- [33] A. Gregor, E. Kostrzewska, W. Godorowska, *Infusionsther. Klin. Ernaehr. - Forsch. Prax.* **1977**, 4, 48.
- [34] Z. Cai, A. Sasmal, X. Liu, S. A. Asher, *ACS Sens.* **2017**, 2, 1474.
- [35] K. V. Abhinav, M. Vijayan, *J. Macromol. Sci., Part A: Pure Appl. Chem.* **2014**, 86, 1335.
- [36] J. T. Zhang, Z. Cai, D. H. Kwak, X. Liu, S. A. Asher, *Anal. Chem.* **2014**, 86, 9036.
- [37] A. J. Kalb, A. Levitzki, *Biochem. J.* **1968**, 109, 669.
- [38] A. Battigelli, J. H. Kim, D. C. Dehigaspitiya, C. Proulx, E. J. Robertson, D. J. Murray, B. Rad, K. Kirshenbaum, R. N. Zuckermann, *ACS Nano* **2018**, 12, 2455.
- [39] J. Seo, B. C. Lee, R. N. Zuckermann, *Compr. Biomater. II* **2017**, 2, 41.
- [40] Y.-J. Choi, T. Takahashi, M. Taki, K. Sawada, K. Takahashi, *Biosens. Bioelectron.* **2021**, 172, 112778.
- [41] S. Patra, E. Roy, R. Madhuri, P. K. Sharma, *Nanobiosensors*, Elsevier, Amsterdam **2017**, pp. 713–772.
- [42] D. Dupont, in *Encyclopedia of Dairy Sciences*, Elsevier, Amsterdam **2022**, pp. 400–404.
- [43] W. Ensinger, M. Ali, S. Nasir, I. Duznovic, C. Trautmann, M. Eugenia Toimil-Molares, G. R. Distefano, B. Laube, M. Bernhard, M. Mikosch-Wersching, H. F. Schlaak, M. El Khoury, in *World Congress on Recent Advances in Nanotechnology*, **2017**.

- [44] M. Trujillo, B. Alvarez, J. M. Souza, N. Romero, L. Castro, L. Thomson, R. Radi, *Nitric Oxide* **2010**, 61, <https://doi.org/10.1016/b978-0-12-373866-0.00003-4>.
- [45] G. Fanali, A. Di Masi, V. Trezza, M. Marino, M. Fasano, P. Ascenzi, *Mol. Aspects Med.* **2012**, 33, 209.
- [46] G. Wang, F. Zhu, T. Lang, J. Liu, Z. Hong, J. Qin, *Nanoscale Res. Lett.* **2021**, 16, 109.
- [47] D.-K. Lee, J.-H. Kang, J. Kwon, J.-S. Lee, S. Lee, D. H. Woo, J. H. Kim, C.-S. Song, Q.-H. Park, M. Seo, *Sci. Rep.* **2017**, 7, 8146.
- [48] D. Cheng, X. He, X. Huang, B. Zhang, G. Liu, G. Shu, C. Fang, J. Wang, Y. Luo, *Int. J. RF Microw. Comput.-Aided Eng.* **2018**, 28, e21448.
- [49] K. Liu, R. Zhang, X. Chen, E. Pickwell-Macpherson, in *Int. Conf. on Infrared, Millimeter, and Terahertz Waves (IRMMW-THz)*, IEEE, Piscataway, NJ **2018**, vol. 2018-Sept.
- [50] W. Xu, L. Xie, J. Zhu, X. Xu, Z. Ye, C. Wang, Y. Ma, Y. Ying, *ACS Photonics* **2016**, 3, 2308.
- [51] S. Yan, L. Xia, D. Wei, H. L. Cui, C. Du, in *IEEE 3M-NANO 2016 –6th IEEE Int. Conf. on Manipulation, Manufacturing and Measurement on the Nanoscale*, IEEE, Piscataway, NJ **2017**, pp. 327–330.
- [52] J. Zhou, X. Zhao, G. Huang, X. Yang, Y. Zhang, X. Zhan, H. Tian, Y. Xiong, Y. Wang, W. Fu, *ACS Sens.* **2021**, 6, 1884.
- [53] W. Bode, D. Turk, A. Karshikov, *Protein Sci.* **1992**, 1, 426.
- [54] K. Hilpert, J. Ackermann, D. W. Banner, A. Gast, K. Gubernator, P. Hadvary, L. Labler, K. Mueller, G. Schmid, T. B. Tschopp, H. Van De Waterbeemd, *J. Med. Chem.* **1994**, 37, 3889.
- [55] Y.-L. Ying, Z.-L. Hu, S. Zhang, Y. Qing, A. Fragasso, G. Maglia, A. Meller, H. Bayley, C. Dekker, Y.-T. Long, *Nat. Nanotechnol.* **2022**, 17, 1136.
- [56] S. Acharya, A. Jiang, C. Kuo, R. Nazarian, K. Li, A. Ma, B. Siegal, C. Toh, J. J. Schmidt, *ACS Sens.* **2020**, 5, 370.
- [57] A. Soltani, D. Jahn, L. Duschek, E. Castro-Camus, M. Koch, W. Withayachumnankul, *IEEE Trans. Terahertz Sci. Technol.* **2016**, 6, 32.
- [58] R. P.-A. Berntsson, S. H. J. Smits, L. Schmitt, D.-J. Slotboom, B. Poolman, *FEBS Lett.* **2010**, 584, 2606.
- [59] O. Keskin, R. L. Jernigan, I. Bahar, *Biophys. J.* **2000**, 78, 2093.
- [60] M. Bernhard, M. Diefenbach, M. Biesalski, B. Laube, *ACS Sens.* **2020**, 5, 234.
- [61] M. Klimek-Ochab, A. Mucha, E. Zymanczyk-Duda, *Curr. Microbiol.* **2014**, 68, 330.
- [62] R. J. Ouellette, J. D. Rawn, in *Organic Chemistry: Structure, Mechanism, and Synthesis*, Elsevier, Amsterdam **2014**, pp. 907–951.
- [63] H. F. Oldenkamp, J. E. Vela Ramirez, N. A. Peppas, *Regen. Biomater.* **2019**, 6, 1.
- [64] S.-I. Hakomori, *Pure Appl. Chem.* **1991**, 63, 473.
- [65] M. Elsherif, M. U. Hassan, A. K. Yetisen, H. Butt, *ACS Nano* **2018**, 12, 2283.
- [66] C. Chen, Z.-Q. Dong, J.-H. Shen, H.-W. Chen, Y.-H. Zhu, Z.-G. Zhu, *ACS Omega* **2018**, 3, 3211.
- [67] S. Soylemez, B. Yoon, L. Toppare, T. M. Swager, *ACS Sens.* **2017**, 2, 1123.
- [68] J. Soto, T. Hughes, Y. S. Li, *ACS Omega* **2019**, 4, 18312.
- [69] S.-K. Kim, C. Jeon, G.-H. Lee, J. Koo, S. H. Cho, S. Han, M.-H. Shin, J.-Y. Sim, S. K. Hahn, *ACS Appl. Mater. Interfaces* **2019**, 11, 37347.
- [70] X. Yan, X. K. Xu, H.-F. Ji, *Anal. Chem.* **2005**, 77, 6197.
- [71] M. Mesch, C. Zhang, P. V. Braun, H. Giessen, *ACS Photonics* **2015**, 2, 475.
- [72] Q. Dou, Z. Zhang, Y. Wang, S. Wang, D. Hu, Z. Zhao, H. Liu, Q. Dai, *ACS Appl. Mater. Interfaces* **2020**, 12, 34190.
- [73] A. Navale, in *Molecular Nutrition Carbohydrates*, Elsevier, Amsterdam **2019**, pp. 21–34.
- [74] G. W. von Rymon Lipinski, in *Optimising Sweet Taste in Foods*, Elsevier, Amsterdam **2006**, pp. 252–280.
- [75] P. Saeedi, P. Salpea, S. Karuranga, I. Petersohn, B. Malanda, E. W. Gregg, N. Unwin, S. H. Wild, R. Williams, *Diabetes Res. Clin. Pract.* **2020**, 162, 108086.
- [76] S. Tsalamandris, A. S. Antonopoulos, E. Oikonomou, G.-A. Papamikroulis, G. Vogiatzi, S. Papaioannou, S. Deftereos, D. Tousoulis, *Eur. Cardiol.* **2019**, 14, 50.
- [77] K. A. Johnson, B. A. Kroa, T. Yourey, *J. Chem. Educ.* **2002**, 79, 74.
- [78] S. Takahashi, J. I. Anzai, *Langmuir* **2005**, 21, 5102.
- [79] M. Deng, G. Song, K. Zhong, Z. Wang, X. Xia, Y. Tian, *Sens. Actuators, B* **2022**, 352, 131067.
- [80] J. Handley, *Anal. Chem.* **2001**, 73, 225.
- [81] Y.-N. Shi, Y.-J. Liu, Z. Xie, W. J. Zhang, *Chin. Med. J.* **2021**, 134, 1276.
- [82] J.-M. Schwarz, S. M. Noworolski, M. J. Wen, A. Dyachenko, J. L. Prior, M. E. Weinberg, L. A. Herrera, V. W. Tai, N. Bergeron, T. P. Bersot, M. N. Rao, M. Schambelan, K. Mulligan, *J. Clin. Endocrinol. Metab.* **2015**, 100, 2434.
- [83] J. J. Belbruno, *Chem. Rev.* **2018**, 119, 94.
- [84] R. Rajkumar, A. Warsinke, H. Möhwald, F. W. Scheller, M. Katterle, *Talanta* **2008**, 76, 1119.
- [85] G. Wulff, S. Schauhoff, *J. Org. Chem.* **1991**, 56, 395.
- [86] C. Park, J. Yoon, E. L. Thomas, *Polymer* **2003**, 44, 6725.
- [87] O. A. Abd El-Aziz, H. A. Elsayed, M. I. Sayed, *Appl. Opt.* **2019**, 58, 8309.
- [88] Z. Liu, H. Sun, Y. Li, J. Zhang, C. Z. Ning, in *CLEO: Science and Innovations*, San Jose, California United States **2015**, pp. 10–15.
- [89] Z. Cai, J. T. Zhang, F. Xue, Z. Hong, D. Punihale, S. A. Asher, *Anal. Chem.* **2014**, 86, 4840.
- [90] H. N. Umh, S. Yu, Y. H. Kim, S. Y. Lee, J. Yi, *ACS Appl. Mater. Interfaces* **2016**, 8, 15802.
- [91] M. R. Beaulieu, N. R. Hendricks, J. J. Watkins, *ACS Photonics* **2014**, 1, 799.
- [92] O. B. Ayyub, M. B. Ibrahim, R. M. Briber, P. Kofinas, *Biosens. Bioelectron.* **2013**, 46, 124.
- [93] Y. Yamada, K. Aida, T. Uemura, *Agric. Biol. Chem.* **1966**, 30, 95.
- [94] M. Ameyama, O. Adachi, *Methods Enzymol.* **1982**, 89, 154.
- [95] T. Theophanides, *Int. J. Quantum Chem.* **1984**, 26, 933.
- [96] B. Poljšak, P. Jamnik, P. Raspor, M. Pesti, in *Encyclopedia of Environmental Health*, Elsevier, Amsterdam **2019**, pp. 831–837.
- [97] M. Moustakas, *Materials* **2021**, 14, 549.
- [98] L. Wang, G. Fang, D. Cao, *Sens. Actuators, B* **2015**, 207, 849.
- [99] D. bi Myung, S. Hussain, S. Y. Park, *Sens. Actuators, B* **2019**, 298, 126894.
- [100] H. Tan, S. Y. Park, *ACS Sens.* **2021**, 6, 1039.
- [101] Z. A. Othman, M. M. Alam, M. Naushad, R. Bushra, *Int. J. Electrochem. Sci.* **2015**, 10, 2663.
- [102] Y.-H. Chan, Y. Jin, C. Wu, D. T. Chiu, *Chem. Commun.* **2011**, 47, 2820.
- [103] A. A. P. Khan, G. C. Bazan, B. G. Alhogbi, H. M. Marwani, A. Khan, M. M. Alam, M. M. Rahman, A. M. Asiri, *J. Mater. Res. Technol.* **2020**, 9, 9667.
- [104] Y. Qiao, C. Shi, X. Wang, P. Wang, Y. Zhang, D. Wang, R. Qiao, X. Wang, J. Zhong, *ACS Appl. Mater. Interfaces* **2019**, 11, 5401.
- [105] X. Dong, J. H. Han, C. H. Heo, H. M. Kim, Z. Liu, B. R. Cho, *Anal. Chem.* **2012**, 84, 8110.
- [106] A. Ryabchun, A. Bobrovsky, *Adv. Opt. Mater.* **2018**, 6, 1800335.
- [107] H.-G. Lee, S. Munir, S.-Y. Park, *ACS Appl. Mater. Interfaces* **2016**, 8, 26407.
- [108] E. S. Childress, C. A. Roberts, D. Y. Sherwood, C. L. M. Leguyader, E. J. Harbron, *Anal. Chem.* **2012**, 84, 1235.
- [109] F.-Y. Li, B. Chaigne-Delalande, C. Kanellopoulou, J. C. Davis, H. F. Matthews, D. C. Douek, J. I. Cohen, G. Uzel, H. C. Su, M. J. Lenardo, *Nature* **2011**, 475, 471.
- [110] T. Basu, K. Rana, N. Das, B. Pal, *Beilstein J. Nanotechnol.* **2017**, 8, 762.

- [111] M. Qing, S. Xie, W. Cai, D. Tang, Y. Tang, J. Zhang, R. Yuan, *Anal. Chem.* **2018**, *90*, 11439.
- [112] S. D. Mason, Y. Tang, Y. Li, X. Xie, F. Li, *TrAC, Trends Anal. Chem.* **2018**, *107*, 212.
- [113] S. J. Hurst, A. K. R. Lytton-Jean, C. A. Mirkin, *Anal. Chem.* **2006**, *78*, 8313.
- [114] T. D. Brown, P. D. Dalton, D. W. Hutmacher, *Prog. Polym. Sci.* **2016**, *56*, 116.
- [115] Z. L. Wang, *Annu. Rev. Phys. Chem.* **2004**, *55*, 159.
- [116] M. Faraji, Y. Yamini, A. Saleh, M. Rezaee, M. Ghambarian, R. Hassani, *Anal. Chim. Acta* **2010**, *659*, 172.
- [117] A. Sugunan, C. Thanachayanont, J. Dutta, J. G. Hilborn, *Sci. Technol. Adv. Mater.* **2005**, *6*, 335.
- [118] H. Rafeeq, A. Hussain, A. Ambreen, Zill-E-Huma, M. Waqas, M. Bilal, H. M. N. Iqbal, *J. Nanostr. Chem.* **2022**, *12*, 1007.
- [119] M. B. Gumpu, M. Veerapandian, U. M. Krishnan, J. B. B. Rayappan, *Talanta* **2017**, *162*, 574.
- [120] A. J. F. Griffiths, *An Introduction to Genetic Analysis*, 7th ed., W.H. Freeman, New York, NY **2000**.
- [121] J. D. Watson, F. H. C. Crick, *Nature* **1953**, *171*, 737.
- [122] F. Traversi, C. Raillon, S. M. Benameur, K. Liu, S. Khlybov, M. Tosun, D. Krasnozhan, A. Kis, A. Radenovic, *Nat. Nanotechnol.* **2013**, *8*, 939.
- [123] F. Haque, J. Li, H.-C. Wu, X.-J. Liang, P. Guo, *Nano Today* **2013**, *8*, 56.
- [124] M. Wanunu, J. Sutin, B. McNally, A. Chow, A. Meller, *Biophys. J.* **2008**, *95*, 4716.
- [125] K. J. Freedman, C. W. Ahn, M. J. Kim, *ACS Nano* **2013**, *7*, 5008.
- [126] S. Hernández-Ainsa, N. A. W. Bell, V. V. Thacker, K. Göpflich, K. Misiunas, M. E. Fuentes-Perez, F. Moreno-Herrero, U. F. Keyser, *ACS Nano* **2013**, *7*, 6024.
- [127] L. Liu, H.-C. Wu, *Angew. Chem.* **2016**, *128*, 15440.
- [128] N. C. Seeman, *J. Theor. Biol.* **1982**, *99*, 237.
- [129] S. Dey, C. Fan, K. V. Gothelf, J. Li, C. Lin, L. Liu, N. Liu, M. A. D. Nijenhuis, B. Saccà, F. C. Simmel, H. Yan, P. Zhan, *Nat. Rev. Methods Primers* **2021**, *1*, 13.
- [130] A. B. Farimani, P. Dibaieinia, N. R. Aluru, *ACS Appl. Mater. Interfaces* **2017**, *9*, 92.
- [131] D. Sulaiman, P. Cadinu, A. P. Ivanov, J. B. Edel, S. Ladame, *Nano Lett.* **2018**, *18*, 6084.
- [132] K. Briggs, G. Madejski, M. Magill, K. Kastritis, H. W. De Haan, J. L. McGrath, V. Tabard-Cossa, *Nano Lett.* **2018**, *18*, 660.
- [133] Z. Tang, Z. Liang, B. Lu, J. Li, R. Hu, Q. Zhao, D. Yu, *Nanoscale* **2015**, *7*, 13207.
- [134] A. H. Squires, J. S. Hersey, M. W. Grinstaff, A. Meller, *J. Am. Chem. Soc.* **2013**, *135*, 16304.
- [135] A. Baeissa, N. Dave, B. D. Smith, J. Liu, *ACS Appl. Mater. Interfaces* **2010**, *2*, 3594.
- [136] X. Zhang, X. Peng, S. W. Zhang, in *Science and Principles of Biodegradable and Bioresorbable Medical Polymers: Materials and Properties*, Woodhead Publishing, Cambridge, UK **2017**, pp. 1–33.
- [137] A. Karmi, G. P. Sakala, D. Rotem, M. Rechtes, D. Porath, *ACS Appl. Mater. Interfaces* **2020**, *12*, 14563.
- [138] M. Geissler, L. Malic, K. J. Morton, L. Clime, J. Daoud, J. A. Hernández-Castro, N. Corneau, B. W. Blais, T. Veres, *Anal. Chem.* **2020**, *92*, 7738.
- [139] G. A. Diaz-Quijada, R. Peytavi, A. Nantel, E. Roy, M. G. Bergeron, M. M. Dumoulin, T. Veres, *Lab Chip* **2007**, *7*, 856.
- [140] C. L. Haynes, A. D. McFarland, R. P. Van Duyne, *Anal. Chem.* **2005**, *77*, 338.
- [141] L. Fabris, M. Dante, G. Braun, S. J. Lee, N. O. Reich, M. Moskovits, T.-Q. Nguyen, G. C. Bazan, *J. Am. Chem. Soc.* **2007**, *129*, 6086.
- [142] R. Antiochia, L. Gorton, *Sens. Actuators, B* **2014**, *195*, 287.
- [143] J. Movilli, R. W. Kolkman, A. Rozzi, R. Corradini, L. I. Segerink, J. Huskens, *Langmuir* **2020**, *36*, 4272.



Litzzy L. García-Faustino obtained her B.S. degree at Universidad de las Americas Puebla in 2022. Then she joined the School of Engineering and Sciences at Tecnológico de Monterrey as a Master's student. Her current research work interests are in the fields of material science and nanostructured materials.



Stephen M. Morris received his Ph.D. in engineering from the University of Cambridge. He is now a professor at the Engineering Science Department at the University of Oxford. He is the head of the Soft Matter Photonics Research Group. His current research work focuses on creating novel optoelectronic devices and components using flexible materials like liquid crystals and polymers.



Steve J. Elston received his Ph.D. at Exeter University. His current research work focuses on liquid crystal materials and their diverse applications. He is currently a professor at the Engineering Science Department at the University of Oxford. His research interests are mainly in the field of novel liquid crystal materials and applications, within which he undertakes both theoretical and experimental work.



Yunuen Montelongo received his Ph.D. at the University of Cambridge in 2015. Currently, he is a research fellow in the Department of Engineering Science and Research at Wolfson College. His current work focuses on the theoretical exploration of light–matter interactions, along with practical demonstrations utilizing nanostructured materials.